https://doi.org/10.5194/egusphere-2026-3779
Preprint. Discussion started: 7 July 2026

Century-scale impacts of ice-sheet model initialization on Amundsen Sea Embayment, West Antarctica

Daniel N. Goldberg[1], Paul R. Holland[2], and Kaitlin A. Naughten[2]

[1]School of GeoSciences, University of Edinburgh, Edinburgh, UK
[2]British Antarctic Survey, Cambridge, United Kingdom

Correspondence: D N Goldberg (dan.goldberg@ed.ac.uk)

Abstract. The glaciers of the Amundsen Sea Embayment (ASE) are some of the fastest-thinning in Antarctica. Future ice loss from this region depends on the trajectory of ocean warming. However, the response of glaciers to this warming depends to some extent on how they are initialised, or calibrated, to match observations. The relative importance of these dual factors of forcing and initialisation remains poorly understood. We carry out climate scenario-forced, synchronously coupled ice-ocean simulations of the ASE extending to the 23rd century. We conduct four experiments varying ice-sheet initialisation method (Snapshot versus Transient Calibration) and far-field ocean forcing (baseline climatology versus an RCP8.5 scenario). We find that the mode of ice-sheet initialisation dominates the trajectory of Thwaites Glacier volume loss throughout the 21st century, while climate forcing emerges as the primary control in subsequent centuries — a contrast explained by the low buttressing of Thwaites ice shelf prior to substantial grounding-line retreat. Under RCP8.5 forcing, Thwaites alone contributes up to 2.6 mm/a sea-level equivalent by 2200 following its retreat past Upper Thwaites Ridge, with the full ASE exceeding 3.2 mm/a. Under current ocean conditions, loss rates stabilise near 1.7 mm/a, partly due to growth of pinning points due to a thicker ice shelf compared to RCP8.5. Our results suggest that ASE ice loss remains sensitive to climate forcing even after retreat into the deep interior, implying that emissions mitigation could delay the trajectory of sea-level rise from this region – but that the effects of mitigation would not be felt for nearly a century.

1 Introduction

The glaciers in the Amundsen Sea Embayment (ASE) stand out among Antarctic glaciers in terms of high rates of mass loss and grounding-line retreat (Shepherd et al., 2019; Rignot et al., 2019; Scheuchl et al., 2016; Milillo et al., 2019), high velocities (Rignot et al., 2011; Gardner et al., 2018), and strong ocean-driven melt rates and ice-shelf thinning (Adusumilli et al., 2020; Gourmelen et al., 2025; Dutrieux et al., 2014; Jenkins et al., 2018; Paolo et al., 2015; Davison et al., 2023). From 1992 to 2017, Pine Island and Thwaites Glaciers, the two largest glaciers in the ASE, together contributed approximately 4 mm sea level rise (Shepherd et al., 2019), and instantaneous melt rates in excess of 100 m/a were inferred under some regions of the Thwaites ice shelf (Milillo et al., 2019; Gourmelen et al., 2025).

The high rates of ice loss are in large part due to the loss of ice-shelf buttressing associated with ice-shelf thinning (Shepherd et al., 2004; Pritchard et al., 2012; Reese et al., 2018b), although calving is thought to play an important role (Joughin et al.,

https://doi.org/10.5194/egusphere-2026-3779
Preprint. Discussion started: 7 July 2026

2021). The high melt rates, in turn, are caused by warm Circumpolar Deep Water (CDW) intrusions on the continental shelf through deep bathymetric troughs (Walker et al., 2013; Wåhlin et al., 2010), driven by an along-slope undercurrent (Haigh et al., 2026). It seems likely that CDW will increase on the Amundsen continental slope in the future: regional ocean models forced by output from global coupled climate projections (Taylor et al., 2012) show warming temperatures on the ASE continental shelf (Jourdain et al., 2022; Naughten et al., 2023a; Turner et al., 2025). Moreover, Naughten et al. (2023a), using a large ensemble of ocean model runs forced by output from a coupled climate model (Kay et al., 2015), saw no significant difference in the level of warming between the RCP 8.5 scenario and one in which a 2°C warming target is met – meaning such warming is potentially unavoidable, at least in the 21st century.

Neither of the above studies examined the impact of this warming – or that of the differential levels of warming under different pathways – on grounded ice-sheet loss. To do so requires representation of ice-sheet physics, since the inland response to ice-shelf removal depends on the stress state of the ice sheet-ice shelf system (Fürst et al., 2015; Reese et al., 2018a; Goldberg et al., 2019; Gudmundsson et al., 2023). Moreover, the thinning of ice shelves and retreat of grounding lines can modify ocean-driven melt in a number of ways, such as (i) changing the depth of the ice-shelf base and hence the extent of exposure to warmer waters; (ii) allowing new pathways for CDW to reach the grounding line; and (iii) altering ocean circulation within or near cavities, leading to stronger currents and more efficient "flushing" of cold melt water (Holland et al., 2023). Of these, (i) can be represented somewhat by using a depth-based parameterisation for melt in a dynamic ice model (Cornford et al., 2020), but (ii) and (iii) pose feedbacks that require a fully coupled model of ice and ocean dynamics (De Rydt and Naughten, 2024).

Glaciological theory suggests a positive feedback where a marine ice sheet overlies an inland-deepening bed that could lead to rapid, irreversible ice loss (the Marine Ice Sheet Instability; Weertman, 1974; Schoof, 2007), and ice-sheet simulations with parameterised melt suggest this could lead to catastrophic loss from the ASE sector within several centuries (Joughin et al., 2014; Seroussi et al., 2024). It is therefore critical to study the effects of warming with coupled ice-ocean modeling, as the interactions described above could either slow or accelerate this process.

Coupling of ocean and ice-sheet models, however, introduces a question of how the ice-sheet model should be initialised. The ice sheet is not in steady state at the start of the coupled simulation, and any inherent model trends could strongly influence coupled evolution, at least initially. Using a coupled ice-ocean model of Smith Glacier, an ASE glacier to the west of Thwaites, Goldberg and Holland (2022) showed that the mode of initialisation of the ice model initially had a larger impact on rates of ice loss than climate forcing, but after 2-3 decades, climate forcing mattered more. This result would suggest that initialisation is unimportant for century-scale coupled simulation – though this could be a function of the specific domain studied. Lowry et al. (2021) argues that for Antarctic ice loss, different emissions scenarios do not differentiate within the 21st century. One might expect, therefore, that the relative influence of climate and initial state may not "cross over" on this time scale either when examining larger domains – but this has not been tested.

In this study, we carry out coupled ice sheet-ocean simulations of the ASE into the 23rd century. We vary the method of coupled model initialisation, based on the observations used to constrain the dynamic parameters of the ice-sheet model (velocities and surface elevation change, or velocities alone). We also vary the far-field ocean forcing between present levels, and those based on climate model outputs generated under an SSP5-85 scenario (Seroussi et al., 2024), for a total of four

https://doi.org/10.5194/egusphere-2026-3779
Preprint. Discussion started: 7 July 2026

multi-century experiments. We observe varying responses across the major ASE glaciers: Smith has short-lived dependence on initialisation (in line with Goldberg and Holland, 2022), while Thwaites ice loss is determined by initialisation well into the 22nd century, with Pine Island in between. Our results also comprise the first high-resolution, multi-century coupled ice-ocean simulation of the ASE forced by projected climate change, and give insight into the pathways through which ice loss may occur.

2 Methods

Given nonstandard use of two models and their coupling, we describe here our ocean modelling methodology, ice-sheet modelling methodology, and coupling methodology. We describe all data sources within the appropriate subsection.

2.1 Ocean Modelling

We use the MITgcm (Marshall et al., 1997), which has been adapted for circulation within ice-shelf cavities (Losch and Heimbach, 2007; Dansereau et al., 2014). Furthermore, we use a version of the code which allows online evolution of the cavity geometry, which is important for ice-ocean coupling; details are given below.

2.1.1 Model domain and geometry

The ocean domain includes the cavities of Thwaites, Pine Island and Smith, and extends $\sim$ 100 km past the ice shelves (Fig. 1). A Cartesian mesh is used within a polar stereographic projection, with a uniform resolution of 1250 m over most of the domain (see Sec. 2.2). Vertical resolution is 25 m, with a z-vertical coordinate system. At the ocean-facing lateral boundaries, we impose temperature, salinity, and velocity from monthly files. These boundary files are described in Section 2.1.2.

The bathymetry and ice base used by the ocean (and ice) model is based on BedMachine-Antarctica v3 (Morlighem et al., 2020a; Morlighem, 2022). However, models of ice-ocean interaction often underestimate deep melt rates for Pine Island, potentially because BedMachine bathymetry is too shallow in its cavity. Bett et al. (2024) addressed this by deepening bathymetry (only where ice is floating according to BedMachine) to allow a minimum depth of the ocean column at C-grid locations. In their study they deepened by up to 280 m throughout the entire domain; in this study, we deepen by at most 100 m (which is within the uncertainty of the under-ice shelf BedMachine bathymetry) and only within the Pine Island cavity.

2.1.2 Downscaling of forcings

To obtain boundary forcings, we use outputs of two regional models: (i) the regional model of Naughten et al. (2023a), which was forced by an ensemble of CESM1 simulations under the RCP 8.5 scenario to 2100; and (ii) the RCP 8.5 scenario of the Community Earth System Model (CESM2-WACCM), run to 2300. The latter was provided through the ISMIP6-2300 protocol (Seroussi et al., 2024).

https://doi.org/10.5194/egusphere-2026-3779
Preprint. Discussion started: 7 July 2026

Monthly files of boundary condtions are generated from these products. The temperature and boundary conditions T_{bound} in year y and month m can be described as:

$$T_{bound}(y,m) = T_N^{(clim)}(m) + (T_{CESM2}(y,m) - T_{CESM2,0}). \quad (1)$$

Here $T_N^{(clim)}$ is a monthly climatology of the Naughten ensemble mean for the period 2000-2010, and $T_{CESM2}(y,m)$ is CESM2 temperature. The latter is provided annually, therefore it is interpolated linearly in time to the appropriate month in the calculation above. $T_{CESM2,0}$ corresponds to 2005, taken as the nominal year of the Naughten climatology. All terms on the right hand side are spatially interpolated (in the horizontal and vertical) to our ocean model boundary. Boundary salinities ($T_{bound}(y,m)$) are produced similarly. As the ISMIP6-2300 forcings only provide temperature and salinity we use velocities from the Naughten ensemble mean to 2100. Since a noticeable trend in velocities is not seen, we use a 2090-2100 monthly climatology of velocity beyond 2100. The temporal change in temperature along the northern and western boundaries is shown in Fig. 2.

The model used by Naughten et al. (2023a) exhibits spurious convection, which could unrealistically cool the continental shelf. The convection is episodic, and occurs in different years in each ensemble member, thus we minimise the effect by averaging over the ensemble. The CESM2-WACCM outputs were selected because the warming at depth on the boundaries of our ocean domain is more modest than in the other climate models selected for ISMIP6-2300. It also is an updated version of the model downscaled by Naughten et al. (2023a) which may provide some level of concordance, but this has not been investigated.

2.1.3 Ice-shelf melt near grounding line

Despite the adjustments to ocean bathymetry above, melt rates remain too low near the grounding line, at least for Pine Island, when using a standard parameterisation for ice-shelf melt and commonly used parameters. The parameterisation of Dansereau et al. (2014) is based on a shear-driven boundary layer (Holland and Jenkins, 1999) in which turbulent mixing is derived from far-field currents. In MITgcm the velocity in the adjacent cell is used, which is related to shear through a frictional drag parameter C_D. In Figs. 3a-c we show mean modelled 2010-2020 melt-depth profiles under Pine Island. In these runs, the ice geometry was held steady, in contrast to the evolving cavities in the coupled runs (Sec. 2.1.4). They are compared against a high-resolution remotely-sensed product for the same period (Gourmelen et al., 2025; Goldberg et al., 2026). With a value of $C_D = 0.006$ (Fig. 3a), values are in rough agreement above 400 m, but underestimate by up to 75% at depth; such a melt field leads to spurious thickening of the ice shelf and advance of the grounding line in a coupled model (not shown). While such a value of C_D is smaller than that found from in-situ measurements on another Antarctic ice shelf (Jenkins et al., 2010), a much larger value of $C_D = 0.014$ (Fig. 3b) still gives values up to 50% too low at depth.

The deficit is likely because model resolution may be too coarse to represent currents in thin ocean columns. A pragmatic approach is taken here: the *exchange velocities* γ_T and γ_S, which facilitate heat and salt transfer at the ice-ocean interface, are allowed to transition gradually, from the velocity-dependent form of Dansereau et al. (2014) to being directly specified as

https://doi.org/10.5194/egusphere-2026-3779
Preprint. Discussion started: 7 July 2026

constants γ_{T0}, γ_{S0} (Grosfeld et al., 1997). This prevents lowering of melt in regions where currents are limited due to model resolution or unrepresented physics.

Details of this modified melt formulation are given in Reed et al. (2026). In that work, the authors carry out an optimisation of parameters through comprehensive statistical sampling using a coupled ice-ocean ensemble, whereas in this work we choose parameters heuristically, based on a small number of samples with a static ice-shelf simulation. Our selected parameters are $C_D = 0.006$ and $\gamma_{T0} = 1.2 \times 10^{-4}$ (γ_{S0} is set based on a fixed ratio in MITgcm). As shown in Fig. 3c this results in an improved profile. We choose our transition depth such that melt is completely independent of ocean velocity for column thickness below 100 m, since smaller transition depths give less favorable results (not shown). Our modified melt formulation and chosen parameters lead to shelf-wide melt estimates larger than those observed; this is likely due to small overestimates at shallow depths, which cover a larger area (Fig. 3d). Since our priority is accurate melt rates in regions most important to the grounded ice, such as near the grounding line, this is acceptable for the present study.

2.1.4 Evolving ocean geometry

We use a version of MITgcm modified to allow for synchronous changes in ice shelf base (Jordan et al., 2017; Gadi et al., 2023) and grounding line (Goldberg et al., 2018; Bett et al., 2024). The upper surface changes at the ocean time step in response to changes in ice shelf mass in mass-, heat- and salt-conservative fashion. Grounding line change is facilitated by maintaining a thin ocean layer (∼2 m) under grounded ice. When grounded ice thins, this layer can then inflate naturally as water flows in to equalise the ocean pressure. A conservative porous flux parameterisation facilitates this flow in the case where is no pathway within the ocean domain for water to move into the new cavity.

The synchronous approach means that heat and salt do not need to be added or removed heuristically to newly formed ocean cells when the cavity grows, and currents need not be adjusted to conserve barotropic transport and avoid shocks (De Rydt and Naughten, 2024). There are drawbacks as well: as we do not "dig" the bathymetry like some ice-ocean models in order to impose minimum ocean columns (Yung et al., 2026), strong currents can arise in very thin ocean columns, for instance near ice-shelf pinning points, which can become unstable. To prevent this, we introduce a new scaling of the quadratic bottom drag coefficient C_{BD} :

$$C_{BD} = \alpha C_{BD,0} + (1-\alpha) C_{BD,max}, \quad \alpha = \frac{1}{2}\left(1 + \tanh\left(\frac{D - D_{drag}}{D_{drag}/4}\right)\right), \tag{2}$$

where C_{BD} is the bottom drag coefficient for thick ocean columns. With a value of 37.5 m for D_{drag}, bottom drag is increased relative to thick columns when the column depth is below 50 m, reaching a maximum below 25 m. A value of $C_{BD,max}$ ten times that of C_{BD} is used, which ensures stability in these regions.

The coupling approach also means that as grounded ice is lost, the sea level within the domain rises strongly due to fixed velocities on the boundaries. To counter this, we add an outflowing barotropic velocity at the boundaries equal to $\eta/\Delta t$, where η is mean open-ocean sea level relative to a reference zero state and Δt is the ocean time step (Snow et al., 2017). It is a similar mechanism to that ensuring that imposed boundary velocities do not add or remove volume, commonly used in MITgcm regional configurations.

https://doi.org/10.5194/egusphere-2026-3779
Preprint. Discussion started: 7 July 2026

2.2 Ice-sheet modelling

We use STREAMICE, the ice-sheet component of MITgcm (Goldberg and Heimbach, 2013). It solves the higher-order DIVA balance (Goldberg, 2011; Lipscomb et al., 2019; Robinson et al., 2022) using a mixed finite element-finite volume method on a rectangular grid. The extent of the domain is shown in Fig. 1; the model captures most of the flow catchments of Thwaites and Pine Island Glaciers, and all of Smith. Mesh resolution is 1250 m for the region $x < -1400$ km and $y < -120$ km. Beyond these locations, the mesh "accordions" outward similarly to Barnes et al. (2021), with a maximum spacing of ∼2.5 km.

STREAMICE implements the regularized-Coulomb friction sliding law of Cornford et al. (2020):

$$\boldsymbol{\tau}_b = -\frac{\alpha^2 \beta^2 N |\boldsymbol{u}|^{1/m}}{\left(\beta^{2m}|\boldsymbol{u}| + (\alpha^2 N)^m\right)^{1/m}} |\boldsymbol{u}|^{-1} \boldsymbol{u} \tag{3}$$

where $\boldsymbol{\tau}_b$ is basal drag; $\boldsymbol{u}$ is sliding velocity; and N is effective pressure – which is set assuming water pressure is hydraulically connected to the ocean. As in Cornford et al. (2020), $m = 3$. In general, Eq. 3 asymptotes to a Coulomb-plastic sliding law within ∼10 km of the grounding line, while further inland it is similar to Weertman-type sliding (Joughin et al., 2019; Goldberg et al., 2026). β is in general spatially varying, as is $\overline{B}$, the coefficient of the strain-rate invariant in Glen's flow law (Glen, 1955; Cuffey and Paterson, 2010) that determines the nonlinear viscosity.

2.2.1 Snapshot calibration

Marine ice-sheet models requite initialisation to ensure they have reasonable sensitivities and responses to climate forcing. A common approach is to calibrate the constitutive parameter fields β and $\overline{B}$ based on satellite-inferred velocities with a given bed and thickness. The method proceeds by defining a *cost function* (Morlighem and Goldberg, 2023) that penalises misfit with observations, while also limiting nonphysical spatial variations in the parameters (the latter is called regularisation). Such a calibration is often referred to as "snapshot" since it does not involve time-dependence. Our snapshot calibration is based on that of Barnes et al. (2021) and Goldberg and Holland (2022). BedMachine geometry is imposed and MEaSUREs velocities (Rignot et al., 2017) are used for calibration. The initial guess for $\overline{B}$ follows from the temperature solution of Van Liefferinge and Pattyn (2013), and deviations from this field over grounded ice are penalised. Regularisation parameters for β and $\overline{B}$ follow from Goldberg et al. (2019).

2.2.2 Transient calibration

Since glacial flow is non-inertial, i.e. the motion does not depend on its history, a snapshot calibration should in theory provide a reasonable dynamic representation of the ice sheet. Observational errors and temporal mismatch of thickness and velocity, however, can lead to spurious dynamic behaviour (Goldberg et al., 2015; Goldberg and Holland, 2022; Badgeley et al., 2025; Goldberg et al., 2026). Therefore we carry out an additional calibration ("transient" calibration), in which the cost function is based on the output of a time-evolving model and has an added term to penalise misfit of surface elevation change with observations.

https://doi.org/10.5194/egusphere-2026-3779
Preprint. Discussion started: 7 July 2026

The procedure is based on that of Goldberg and Holland (2022). The ice model is run from 2013 (the nominal date of BedMachine) until 2018, and the mean surface elevation change rate is compared with that of Shepherd et al. (2019), a radar-based 5 km product that covers Antarctica. Velocity misfit with MEaSUREs is calculated after 1 year (as opposed to the initial velocity or velocity after 5 years); this is in order to use a date within the product's temporal range (1996-2016), while also allowing for sub-annual adjustment due to temporal data mismatch of data sources. During the 5-year calibration window the model is forced by the time-mean melt rate field generated with our selected parameters (Sec. 2.1.3) and the same surface mass-balance field as the coupled model (Sec. 2.3). As in the snapshot calibration, optimal parameter fields are found iteratively; snapshot-derived parameter fields serve as initial guesses. We limit the elevation change calibration region to grounded ice, and further to where thinning rate is greater than 0.5 m/a (*cf* a threshold of 1.0 m/a in Goldberg and Holland, 2022), to ensure we are capturing signals of dynamic change.

Results of the calibration are shown in Fig. 4. The snapshot calibration yields an initial velocity field that matches well with observations (Figs. 4d,e) but leads to spurious thickening in the trunk of Pine Island and excessive thinning on Thwaites over the next 5 years (Figs. 4a,b). One year into the transient calibration, velocities are broadly similar to the observed values, with the largest different being low velocities on the Thwaites western ice shelf (Figs. 4d,f), which could be due to ice-shelf thinning. In terms of 5-year elevation change, however, far better agreement with observations is seen with transient calibration (Figs. 4b,c), with the correct level of thinning on all glaciers. Each calibration experiment produces a (β,$\overline{B}$) pair which provides ice inputs in the appropriate coupled simulation.

We note that some snapshot approaches include a cost term that penalises misfit with observed thinning rates (e.g., Arthern et al., 2015; De Rydt and Naughten, 2024), which may or may not be followed by a timd-dependent "relaxation" that is meant to further ensure a transient state consistent with observations van den Akker et al. (2026). We do not include thinning rates in our snapshot cost function, and it is difficult to say how their inclusion would affect the results in Fig. 4b. Still, we present two different calibrations representing commonly used approaches in ice-sheet modeling, in order to determine how important the different approaches are, and for how long.

2.3 Ice-ocean coupling

While STREAMICE and the MITgcm ocean model can run within the same executable on the same grid (as in Goldberg and Holland, 2022), doing so in this study would waste computational resources by solving ocean physics where it is not needed. Instead a newly-developed approach similar to Bett et al. (2024) is used. The model is divided across two executables: one, the *ICE* executable, solves for ice velocities everywhere and evolves ice thickness outside of the *OCEAN* domain (dashed lines in Fig. 1). The *OCEAN* executable evolves ocean dynamics, as well as ice thickness, within the *OCEAN* domain, but does not solve for ice velocities. It evolves ice thickness through an ice-sheet "stub": the STREAMICE code runs within this executable, with ice thickness H updating on the ocean time step according to the mass conservation equation (Cuffey and Paterson, 2010)

$$\frac{\partial H}{\partial t} + \nabla \cdot (H\overline{\boldsymbol{u}}) = \dot{a} - \dot{m} \tag{4}$$

https://doi.org/10.5194/egusphere-2026-3779
Preprint. Discussion started: 7 July 2026

where $\overline{\boldsymbol{u}}$ is the depth-averaged velocity vector, $\dot{a}$ is surface mass balance and $\dot{m}$ is melt rate (positive where melting). Within the "stub", Eq. 4 updates at the ocean time step, with $\dot{m}$ updated at each time step. $\overline{\boldsymbol{u}}$, which is expensive to calculate, is not calculated in the stub but instead copied over from the *ICE* executable and held constant over a given period i.e. the coupling frequency T_{cpl} (which is some integer multiple of the ocean time step).

The coupling scheme proceeds as follows, beginning at an aribitrary time T, where T is a multiple of T_{cpl} from the starting time of the simulation:

1. The *ICE* executable solves for velocity, and evolves thickness over one time step of length T_{cpl}, i.e. from time T to $T+T_{cpl}$, over the whole *ICE* domain. Within this step, $\dot{m}$ is set to zero (as ice-shelf thickness is overwritten, see below).
2. The ice-sheet velocity is extracted and provided as inputs to the *OCEAN* executable; since STREAMICE implements explicit time-stepping, the velocities correspond to ice thickness at time T.
3. In addition, ice thickness at the time T is provided at the boundary of the *OCEAN* grid, to provide a boundary condition for Eq. 4.
4. The *OCEAN* executable then is run from T to $T+T_{cpl}$ on the ocean timestep, beginning from its exact state at T (the end of the previous coupling cycle).
5. The ice-sheet thickness within *OCEAN* at time $T+T_{cpl}$ then replaces ice thickness in *ICE* where the model grids overlap, allowing the *ICE* executable to advance to $T+2\times T_{cpl}$.

An important point about the above scheme is that while the ocean model is stopped and restarted, the coupled evolution is synchronous in that the ocean evolves continuously with ice-sheet geometry. At each coupling step there is a step-change in ice velocity as seen by the OCEAN domain, but the thickness of the ice evolves continuously since the ocean model "owns" the ice thickness within its domain.

A T_{cpl} of 10 days is used in our experiments (in contrast to an ocean time step of 100 s, necessary due to the strong currents and model resolution). Over the coupling period the change in ice thickness is sufficiently small that holding ice velocity constant (within the *OCEAN* domain) is a good approximation, while the computational cost of calculating ice-sheet velocity with this frequency is negligible relative to the cost of the ocean code. (The only reason a smaller T_{cpl} is not used is due to the large number of data files produced.) At the boundary between the ocean domain and the inland ice-sheet domain, there is effectively a discontinuity in the time step of Eq. 4. Discontinuities in ice-sheet thickness and velocities do not arise, so it is assumed that at this location, the time-average of the *OCEAN* solution of Eq. 4 well approximates that of *ICE*.

The inland extent of the ocean model is chosen conservatively based on expected grounding line retreat. In instances where the Thwaites grounding line retreated further than expected, the ocean model was expanded via manipulation of the MITgcm restart files (binary files that encapsulate the model "state") as a one-off process (Fig. 1).

We carry out four experiments in all, based on two modes of ice-sheet calibration: transient or snapshot; and two far-field ocean forcings: bias-corrected CESM2 RCP85 outputs, and "Baseline" forcing i.e. the 2000-2010 climatology from Naugh-

https://doi.org/10.5194/egusphere-2026-3779
Preprint. Discussion started: 7 July 2026

ten et al. (2023a) (Sec. 2.1.2). We will sometimes for brevity refer to these below as e.g. **TCBase**, **Snap85**, for transiently-calibrated, baseline-forced and snapshot-calibrated, RCP85-forced, respectively. In all coupled experiments, ice-sheet surface mass balance, applied to Eq. 4 within both the *ICE* and the *OCEAN* model, is the time-average of Van Wessem et al. (2014), and does not evolve.

As described in Sec. 2.1.4, running an ocean model continously for centuries with arbitrarily evolving geometry makes the model susceptible to numerical instability. Rapid grounding line retreat over complex topography (which is likely in future centuries in the ASE) is expected to cause rapid ice and oecean adjustment. All of our simulations reach a point at which grounded thinning rates are an order of magnitude larger than today with grounding-line retreat rates on the order of tens of kilometers per year, and the associated strong currents and thin ocean columns lead to numerical instability and failure. Despite this, we are able to carry out coupled simulations over multiple centuries and analyse the pathways that lead to this point of strong loss.

2.4 Flow catchments

In our results and analysis it is useful to divide our model domain into separate flow catchments for Pine Island, Thwaites and Smith glaciers (e.g., Fig. 8). In order to do so we use the delineations of Mouginot et al. (2017). For simplicity, however, we combine the Haynes catchment with Thwaites, and our "Smith" catchment is the combined Smith, Pope, and Kohler catchments (together with Crosson and Dotson ice shelves).

3 Results

Volume above Floatation (V_{af}) indicates the ice mass in a domain that will contribute to sea level if it melts (Dupont and Alley, 2005; Greve and Blatter, 2009) and is a common way of examining ice-sheet change over time; this metric is calculated for all four experiments, and for each of the Pine Island, Thwaites, and Smith catchments (Figs. 5a-c). Corresponding rates of change of V_{af} (Figs. 5d-f) and ice-shelf total (area-integrated) melt (Figs. 5g-i) are shown as well.

Each simulation terminates at a different time, with **Snap85** experiencing model failure in ∼2170 and **TCBase** almost a century later. In each catchment, the initial behaviour of each Transiently-calibrated experiment is similar to one another, and similarly for Snapshot-calibrated experiments. This similarity erodes over time, but on very different time scales depending on the catchment. For Smith, by around 2050, $\frac{dV_{af}}{dt}$, the rate of change of V_{af}, for the two RCP85-forced experiments exhibit very similar behavior, which is distinct from the two Baseline experiments (Fig. 5f) – a result consistent with Goldberg and Holland (2022). In contrast, total V_{af} loss and $\frac{dV_{af}}{dt}$ for Thwaites depend very strongly on calibration type, and very weakly on climate forcing, throughout the 21^{st} century (Figs. 5b,e).

In general, for melt rates the dependence on climate emerges earlier relative to that of V_{af} loss – which is not surprising given it is more directly tied to the forcing. This is clear for Pine Island, for instance, where the difference in melt rate between **TC85** and **TCBase** is similar to the difference between **TC85** and **Snap85** from mid-21^{st} century. For Thwaites, the **TC85**-**TCBase** melt difference is relatively small, but non-negligible, during the latter part of 21^{st} century, and similarly for the

https://doi.org/10.5194/egusphere-2026-3779
Preprint. Discussion started: 7 July 2026

Snapshot-calibrated experiments. To make this concept of "emergence" of climate dependence more concrete, we introduce an *emergence* ratio:

$$r_{emerge}(t) = \frac{\Delta_{climate}(t)}{\Delta_{calib}(t)}, \tag{5}$$

where

$$\Delta_{climate}(t) = \frac{1}{2}\Big(\big|(\cdot)_{TC85}(t) - (\cdot)_{TCBase}(t)\big| + \big|(\cdot)_{Snap85}(t) - (\cdot)_{SnapBase}(t)\big|\Big);$$

$$\Delta_{calib}(t) = \frac{1}{2}\Big(\big|(\cdot)_{TC85}(t) - (\cdot)_{Snap85}(t)\big| + \big|(\cdot)_{TCBase}(t) - (\cdot)_{SnapBase}(t)\big|\Big),$$

and the quantity $(\cdot)$ in ellipses can be either V_{af}, rate of change of V_{af}, or melt. In other words, r_{emerge} is the ratio at a certain time of the absolute difference arising from climate (averaged over the types of calibration) to that arising from calibration (averaged over the two forcings). r_{emerge} is plotted up to 2150 for $\frac{dV_{af}}{dt}$ (Fig. 6a) and for melt (Fig. 6b) for each catchment. While there is no definitive threshold to establish the emergence, qualitative differences can be seen in terms of $\frac{dV_{af}}{dt}$. For Smith, the ratio rises above 1 by 2050, whereas aside from a small spike in 2160, the ratio for Thwaites remains $< 25\%$ until 2090. The ratio for Pine Island, while remaining below an arbitrary threshold of 0.75 until after 2100, increases steadily through the 21^{st} century. Meanwhile, for melt, the ratio becomes significant for Thwaites (and other catchments) in the early parts of the 21^{st} century.

Comparing ocean bottom temperatures between Baseline and RCP85-forced simulations suggests a potential reason for the small proportional impact of climate scenario on Thwaites in the 21^{st} century (compared to Pine Island). The difference in bottom temperatures in 2100 between $TC85$ and $TCBase$ are shown in Fig. 7a. While the Pine Island cavity has warmed 2° or more in most places, most of the Thwaites cavity has warmed by 1° or less. This could reflect cooling of CDW as it circulates first through Pine Island cavity and then into Thwaites (Gourmelen et al., 2025). Still, the Thwaites increase in melt due to forcing is not negligible; in 2100, the magnitude of increase is on the order of 2013 melt rates (~60 Gt/a).

After the V_{af} loss rate of Thwaites becomes ~1 mm/a Sea Level Equivalent (SLE) – which happens in ~2120 for the Snapshot-calibrated experiments and ~2150 for the Transient-calibrated ones – the loss rate trajectories are similar for each RCP85-forced experiment independent of calibration type, albeit staggered by three decades. The same is true for the Baseline-forced experiments. All experiments experience a slight decrease in loss rates toward the end of the simulation, seen as a local maximum in the $\frac{dV_{af}}{dt}$ curve. The decreases all correspond to when the grounding line is coincident with Upper Thwaites Ridge (UTR; Fig. 7b, location of ridge Fig. 7a). UTR is noted as a stabilizing feature by Schwans et al. (2023).

After retreating past the ridge, Thwaites exhibits strong acceleration of loss in the RCP85-forced experiments, with the annual loss accelerating at a rate of ~0.3 mm/a^2 SLE, and losing 1000 Gt/a (2.75 mm/a SLE) at the point of model failure. While losses from a single glacier are unprecedented in modern observations, we point out that this rapid ice loss alone does not necessarily indicate the presence of the Marine Ice Sheet Instability, and discuss this point further in Sec. 4.3. The Baseline-forced runs, on the other hand, maintain high loss rates (up to 1.7 mm/a SLE) but do not show such strong acceleration.

https://doi.org/10.5194/egusphere-2026-3779
Preprint. Discussion started: 7 July 2026

It is instructive to examine the spatial details of the differences among the experiments. Melt rate and grounded thinning rate at the point of model failure are shown in Fig. 8. As mentioned, this occurred at different times in each experiment, which limits quantitative comparison between the states, particularly between the Baseline- and RCP85-forced runs. However, we argue below that the Baseline- and RCP85-forced runs are in qualitatively different states, and it is through this lens that they are analysed.

The RCP85-forced runs (Figs. 8c,d) have higher melt rates, and much stronger thinning at the southern grounding line of Thwaites, than the Baseline-forced experiments (Figs. 8a,b) – though in the latter there are very strong thinning rates in the southeast corner of the ice shelf. The grounding line in the Baseline-forced experiments has retreated further at the point of failure than in the RCP85-forced runs, and is coincident with an "Unnamed" inland ridge (Fig. 7a). Importantly, retreat from UTR has not translated to the strong acceleration seen in the RCP85-forced runs; in fact, the steadying of V_{af} loss at 1.7 mm/a SLE precedes retreat to this ridge (not shown). Grounded ice velocities (Fig. 9) are consistent with thinning rates: in the RCP85 experiment (Fig. 9b) there are high speeds along the southern grounding line – nearly 7500 m/a – but in the Baseline experiment (Fig. 9a) they are much smaller in this region.

Fig. 9 also shows grounding line retreat speed. Rather than presenting as temporally equispaced contours (Schwans et al., 2023, e.g.,) we calculate the speed as in Bett et al. (2024), using the quantity

$$\Delta x_{gl}/\Delta t_{gl}, \tag{6}$$

with Δt_{gl} the time from when any of a cell's neighbors goes afloat until that cell goes afloat, and Δx_{gl} is the distance between those cells. In both forcing scenarios, there is slowed retreat over Upper Thwaites Ridge. In the Baseline-forced run, there is very fast retreat in the southeast corner of Thwaites ice shelf prior to (and likely resulting in) model failure. This is likely due to retreat into the deep Byrd Subglacial Basin (Fig. 7, see also Jordan et al., 2010), which does not occur in the RCP85-forced runs, at least prior to model failure.

Fig. 9 only plots results from the Transiently calibrated experiments. This is because in the case of Thwaites and Smith, results are very similar between the initialisation types. The same is not true for Pine Island: the only simulation with significant Pine Island grounding line retreat is **TC85**; the Transiently-calibrated and Snapshot results are qualitatively different, indicating very different trajectories despite the similarities seen in Fig. 5d,g. We note as well that in **SnapBase**, the Pine Island grounding line advances to Jenkins Ridge, which is unlikely even in the absence of warming Reed et al. (2024). Fig. 8 shows that in all experiments, the retreat of Thwaites impinges on the Pine Island catchment; and it is possible that a component of the loss (and melt) in Fig. 5d,g really belongs to Thwaites, which could explain some of the similarity between **TC85** and **Snap85**, and between **TCBase** and **SnapBase**, in Fig. Fig. 5d,g.

https://doi.org/10.5194/egusphere-2026-3779
Preprint. Discussion started: 7 July 2026

4 Discussion

4.1 Ephemeral grounding of Thwaites ice shelf in the Baseline experiments

In the Baseline experiments (**TCBase** and **SnapBase**) there is continued grounding line retreat past Upper Thwaites Ridge, but grounded velocities and thinning are lower along the southern grounding line than in **TC85** and **Snap85** (Figs. 8, 9) and there is not the same sharp acceleration seen in V_{af} loss. Rather, loss rates remain steady for several decades, oscillating around $\sim$1.7 mm/a SLE (Fig. 5). Fig. 10 plots incremental 6-month changes in Thwaites ice shelf speed over the final 12.5 years of the **TCBase** simulation, showing alternating 2-3 year periods of overall acceleration and deceleration. The patterns are not uniform: in the eastern part, acceleration and deceleration seem to nucleate from a region in the southeast of the shelf where several pinning points grow and subside, while there is consistent deceleration in the western part of the ice shelf. The western deceleration is coincident with a growing set of pinning points on the western ice-shelf margin. Pinning points are potentially important in controlling retreat; Bett et al. (2024) found them to be critical in Thwaites' evolution.

The grounded area associated with these pinning points is plotted in Fig. 11. The western complex of regrounding steadily increases in area, while that of the eastern complex oscillates around a decreasing trend. From visual examination, this oscillation does somewhat explain the oscillation in speed over 2268-2274 (Fig. 11a), while the western complex explains the steady deceleration of the western shelf. It is possible this deceleration and the associated back stress is the reason that strong acceleration of loss is not seen, while grounding line retreat continues in the southeast of the ice shelf.

We note that pinning point area alone is not an accurate proxy for back stress, which depends on flow speed and effective stress in areas of contact (and which was unfortunately not saved in our simulation). For this reason, we do not apply rigorous statistical analysis to the Fig. 11 time series. Still, the RCP85-forced simulations do not exhibit similar regrounding (not shown), or such oscillations of V_{af} loss rates. Thus we speculate that the reduced melt rates and associated thicker ice shelf leads to at least temporary stabilisation of loss rates, even after the grounding line retreats past the Upper Thwaites Ridge.

4.2 Persistence of ice-sheet initialisation

Echoing Goldberg and Holland (2022), the relative impacts of ice-sheet initialisation, or calibration, and climate (oceanic) forcing are examined, but here the analysis is formalized (Eq. 5) and expanded to Pine Island and Thwaites. It is found that the impacts of climate emerge relatively quickly (i.e. over 2-4 decades) for Pine Island and Smith, but that calibration strongly determines V_{af} loss for Thwaites throughout the 21^{st} century. The reasons are not immediately clear, as all ice shelves see higher melt when exposed to warmer far-field ocean conditions (Figs. 5g-h). Proportionately, the increase of Thwaites melt is smaller than Pine Island; this is a potential reason for the persistence of initialisation.

But the extent to which grounded ice responds to ice-shelf melt and associated thinning depends on the stress state of the shelf, and this sensitivity can be quantified in the form of a *Buttressing number* (Fürst et al., 2016; Gudmundsson et al., 2023). This number is formed by finding the ratio

$$r_B = \frac{\boldsymbol{n}^T \mathbf{R} \boldsymbol{n}}{\frac{1}{2}\rho_i g (1-\rho_i/\rho_w) H} \tag{7}$$

https://doi.org/10.5194/egusphere-2026-3779
Preprint. Discussion started: 7 July 2026

where H is ice-shelf thickness; ρ_i and ρ_w are ice and ocean densities, respectively; $\boldsymbol{n}$ is the direction in which buttressing is assessed; and $\mathbf{R}$ is the *resistive stress tensor*:

$$R_{ij} = \tau_{ij} + \delta_{ij} \sum_k \tau_{kk}, \tag{8}$$

with τ the horizontal deviatoric stress tensor and δ the Kronecker delta. We adopt the approach of Fürst et al. (2016) by considering the quantity $(1 - r_B)$, and computing it throughout the shelf, not just at the grounding line (as in Gudmundsson et al., 2023). We use modelled velocity as the choice of direction $\boldsymbol{n}$, unlike Fürst et al. (2016) who considered both flow and principal stress directions. While these two measures differ quantitatively, we expect flow-direction buttressing to give a reasonable representation of sensitivity to melt. As explained in Fürst et al. (2016), we expect the Buttressing number $(1 - r_B)$ to go to zero near calving fronts due to the stress boundary condition; and to be close to (or even larger than) 1 where there is strong compression due to buttressing.

Fig. 12 plots $(1 - r_B)$ for the ASE shelves in 2013, 2100, and 2200 in the **TC85** experiment. According to this metric much of upstream Dotson Ice Shelf is buttressed, meaning thinning here will have a larger impact on grounded ice. For Pine Island, buttressing is high in the shear margins; and on Thwaites, buttressing is high in much of the Eastern ice shelf due to its pinning point. Along Thwaites grounding line, buttressing is low. The results are qualitatively similar to other results that use grid-based linear sensitivities to assess levels of buttressing (Goldberg et al., 2019; Gourmelen et al., 2025), and also to the grounding line assessment of Gudmundsson et al. (2023). By 2100, almost all of Pine Island, Dotson and Crosson ice shelves are highly buttressed. Meanwhile, aside from the connection with Pine Island formed in place of the "Piglet" glacier (Chien et al., 2025), buttressing in Thwaites ice shelf is almost uniformly low. By 2200, Thwaites ice shelf has retreated sufficiently that its margins exert significant backstress, and buttressing levels are higher – though they still remain low in the centre of the ice shelf and along the grounding line.

While flow-direction buttressing is only a proxy for the effect of melting on grounded ice, the results suggest low sensitivity of Thwaites to melt in the 21^{st} century. If this is the case, the trajectory of grounded ice loss is controlled largely by ice dynamics upstream of the grounding line. As these dynamics depend more strongly on basal drag, and hence the frictional parameter field, this largely explains the strong influence of initialisation. The result strongly mirrors that of Gudmundsson et al. (2023), where three independent ice-sheet models showed little response to a complete loss of the 2013 ice shelf.

In the 22^{nd} century (and, where appropriate, beyond), the ice shelf plays a more dynamic role, as do differences in climate forcing and melt rates. However, this mechanism assumes an extensive ice shelf that does not weaken over time due to damage or calve away. This issue is addressed further in Sec. 4.4.

We note that while buttressing of Pine Island is found to be considerable, and while the emergence of climate forcing dependence happens relatively early (Fig. 6), calibration type strongly influences grounding line retreat, well past 2100 (Fig. 8). This is due to the strong thickening signal arising from the Snapshot calibration (Fig. 4b), which leads to a fast advance of the grounding line. It is then difficult, irrespective of forcing, for melt to effect retreat.

https://doi.org/10.5194/egusphere-2026-3779
Preprint. Discussion started: 7 July 2026

4.3 The future and stability of Thwaites Glacier

Our simulations are qualitatively in line with previous, ice sheet-only century-scale modelling studies focusing on Thwaites, showing rapid acceleration of loss rates (Joughin et al., 2014) with intermittent stabilisations (Schwans et al., 2023), and insensitivity to changes in ice-shelf thickness prior to 2100 (Gudmundsson et al., 2023). In this sense our simulations give a representation of how the ASE could evolve over the next several centuries, and importantly how this could depend on climate-driven far-field ocean conditions.

Moreover, our study couples ice with ocean physics, comprising the first multi-century climate scenario-forced coupled ice-ocean simulation of the ASE which faithfully represents current ice speeds and thinning rates. Bett et al. (2024) coupled MITgcm with the WAVI ice-sheet model, but forced by persistent ocean states. Their 180-year "warm" state run saw Thwaites losing up to ∼1.6 mm/a SLE before retreating to Upper Thwaites Ridge and slowing to ∼1.2 mm/a; compare with our results of ∼1.8 mm/a slowing to ∼1.6 mm/a over a similar time period in our **TC85** experiment. Given Bett et al. (2024) used a different ice-sheet model and their "warm" far-field profile was cooler than our far-field conditions in our RCP85-forced runs (Figs. 2 and 7 and their Fig. 1), these differences are likely quantitative rather than qualitative. As such our study suggests that, with a number of caveats (see Sec. 4.4), the ASE glaciers could be contributing more than 3.2 mm/a to sea levels by 2200, under a strong greenhouse gas forcing scenario.

The inland deepening bed and widening catchment of Thwaites has led to speculation that Thwaites may be *unstable* (Scambos et al., 2017) – that a point may have been passed already, or will be passed in the near future, such that drainage (or *collapse*) of the entire basin is inevitable, regardless of climate change, or reversal of such change. Hill et al. (2023) found that in its present state, Thwaites is likely not unstable, but Reese et al. (2023) did not rule out a stability threshold being passed within several centuries. Schwans et al. (2023) found that Thwaites exhibits instability once it retreats past Upper Thwaites Ridge. In our study, we find strong acceleration of V_{af} loss after retreat past this point with RCP85 forcing, but a lack of acceleration with Baseline forcing. This is because of a thicker ice shelf in the Baseline case leading to greater buttressing and pinning point nucleation. Our experiments do not extend far enough to know whether, in either scenario, collapse will eventually occur, and thus do not confirm or refute instability. However, they do demonstrate that, even after retreat past an inland obstacle into the deepest and widest parts of the catchment, evolution is not independent of forcing.

4.4 Limitations of study

There are a number of limitations to our study. Firstly, we do not consider changes in surface mass balance, an important mass budget component, when calculating sea level contribution. We consider neither algorithmic uncertainty i.e. uncertainty arising from numerical details; or model uncertainty, which arises from choices of representation of physics (Aschwanden et al., 2021). In terms of the latter, we consider only a single sliding law (Eq. 3), and a bed strength parameter field (β^2) that does not evolve in time. A parameterisation which is relatively new is also used for melt rates where the ocean model cannot represent the complexity of the ice-ocean interface.

https://doi.org/10.5194/egusphere-2026-3779
Preprint. Discussion started: 7 July 2026

In addition, we consider a single realisation of future ocean conditions from a single climate model, which could introduce errors and biase, both inherent to the climate model and through our downscaling. For instance, the bias correction in Sec. 2.1.2 is carried out in z-space, which could introduce spurious heating or cooling if CESM2 and the regional ocean model have differing mixed-layer depths. In the future, such bias-correction should be carried out in $T/S-$space to avoind this (Naughten et al., 2023b).

Still, the limitation that is likely most relevant to future loss and stability is the lack of implementation of ice-shelf calving or weakening due to damage, a point bearing consideration. It would be difficult to represent calving in our synchronously coupled model as each iceberg would need to be tracked and evolved to prevent tsunamis from sudden mass removal (Stern et al., 2017). Nevertheless, as the Thwaites grounding line recedes in our experiments, the ice shelf lengthens, providing buttressing. Ice shelves much longer and wider do exist in Antarctica, but none undergo such high velocities (up to 8 km/a in our experiments) or are exposed to such high melt rates. If the Thwaites ice shelf were to steadily calve away in our experiments, there would likely be far less dependence on climate forcing; but there would also likely be much higher loss rates and faster grounding line retreat.

Ice shelves and ice tongues have been seen to break up when exposed to strong ocean forcing (Holland et al., 2008; Alley et al., 2021). Still, there is not an observed analogue for an ice shelf with 1000+ Gt/a fluxing across its grounding line. Such an ice shelf would be very fast moving, and also very thick: despite high melt rates, strong advective mass fluxes and a deep grounding line prevent strong thinning of the terminus in our experiments. Such a thick ice shelf could limit the calving rate in typically used crevasse-depth calving formulations (Nick et al., 2010; Wilner et al., 2023), and might be more resistant to weakening due to tidal flexure. High velocities could act against calving-based ice-shelf retreat regardless of mechanism. Shear-zone damage, which could potentially lead to ice-shelf breakup (Lhermitte et al., 2020) is driven by concentrated strain rates, generally arising from thinned areas of shelves; again, such a process could be muted by thicker ice. Additionally, damage creation could be offset by advection of less-damaged into the ice shelf (Surawy-Stepney et al., 2023). The Marine Cliff Instability (DeConto and Pollard, 2016; Crawford et al., 2021), thought to precipitate rapid calving of thick ice sheets, has been shown to be muted for future configurations of Thwaites due to strong dynamic thinning and high velocities (Morlighem et al., 2024). Without question, reliable and physically consistent representations of calving and damage are very much needed before the future stability of Thwaites can be assessed. However, we cannot rule out a large, buttressed Thwaites ice shelf in future centuries; and this implies sensitivity to climate forcing, and potential for stabilisation, when it occurs.

5 Conclusions

We carry out coupled ice-ocean experiments for the Amundsen Sea Embayment, and investigate the impacts of climate-driven ocean change and the mode of ice-sheet initialisation. We find the latter to initially be a stronger determinant of ice-sheet evolution and loss, particularly for Thwaites Glacier, where the effects of initialisation outweigh those of climate for nearly a century.

https://doi.org/10.5194/egusphere-2026-3779
Preprint. Discussion started: 7 July 2026

Post-21st century, evolution of Thwaites is more strongly determined by ocean state. Under an RCP85 scenario with a CESM2 realisation, Thwaites loses 2.6 mm/a sea level equivalent (and the entire ASE loses over 3.2 mm/a) by 2200 in both Transiently- and Snapshot-calibrated models. With a forcing unchanged from the early 2000s, loss rates level at 1.7 mm/a SLE in the mid-23rd century, even as the grounding line moves past a stabilising ridge.

This switch from initialisation to climate-forcing sensitivity post-21st century likely arises as the Thwaites ice shelf lengthens through grounding line retreat, and higher levels of buttressing develop. The switch also has implications for mitigation of anthropogenic sea-level rise. To the extent that ocean warming of the continental shelf is reversible, it suggests that collapse of a large portion of the ASE (resulting in 65 cm sea level rise, and an additional 55 cm if Pine Island collapses as well. Morlighem et al., 2020b) could be averted, or at least delayed, through mitigation. But it also suggests that a trajectory resulting from such mitigation will be indistinguishable from that of no action for many generations, which could raise doubts regarding their effectiveness at future times. While this does not argue against climate action, it does mean that confidence in coupled ice-ocean modelling of Antarctic glaciers needs to be improved.

Code and data availability. MITgcm documentation can be found at https://mitgcm.readthedocs.io. MITgcm checkpoint 69c was used Campin et al. (2026) for the ice-sheet model, and the specialised branch Campin et al. (2021) was used for the ocean model. Experiment-specific code, input and scripts, and the model outputs for the figures in this manuscript, can be found in Goldberg (2026). Due to its large size, the full unprocessed set of coupled experiment outputs is not public-facing, but subsets can be transferred on an individual basis as required.

https://doi.org/10.5194/egusphere-2026-3779
Preprint. Discussion started: 7 July 2026

Author contributions. DG and PH conceived of the experiments, and KN provided regional ocean model output as well as insight into downscaling of CMIP data. DG carried out the experiments and analysis, and wrote the manuscript. All authors reviewed and edited the manuscript.

Competing interests. The contact author has declared that none of the authors have any competing interests.

Acknowledgements. DG acknowledges the Natural Environment Research Council (NERC) grant NE/S006796/1 and DG, PH and KN acknowledge NERC grant UKRI-1266. DG used a large language model to generate a first draft of the model abstract based on the manuscript, which then was edited by the author team.

https://doi.org/10.5194/egusphere-2026-3779
Preprint. Discussion started: 7 July 2026

References

Adusumilli, S., Fricker, H. A., Medley, B., Padman, L., and Siegfried, M. R.: Interannual variations in meltwater input to the Southern Ocean from Antarctic ice shelves, Nature geoscience, 13, 616–620, 2020.

Alley, K. E., Wild, C. T., Luckman, A., Scambos, T. A., Truffer, M., Pettit, E. C., Muto, A., Wallin, B., Klinger, M., Sutterley, T., et al.: Two decades of dynamic change and progressive destabilization on the Thwaites Eastern Ice Shelf, The Cryosphere, 15, 5187–5203, https://doi.org/10.5194/tc-15-5187-2021, 2021.

Arthern, R. J., Hindmarsh, R. C. A., and Williams, C. R.: Flow speed within the Antarctic ice sheet and its controls inferred from satellite observations, Journal of Geophysical Research: Earth Surface, 120, 1171–1188, https://doi.org/10.1002/2014JF003239, 2015.

Aschwanden, A., Bartholomaus, T. C., Brinkerhoff, D. J., and Truffer, M.: Brief communication: a roadmap towards credible projections of ice sheet contribution to sea-level, The Cryosphere Discussions, 2021, 1–14, https://doi.org/10.5194/tc-15-5705-2021, 2021.

Badgeley, J. A., Morlighem, M., and Seroussi, H.: Increased sea-level contribution from northwestern Greenland for models that reproduce observations, Proceedings of the National Academy of Sciences, 122, e2411904 122, https://doi.org/10.1073/pnas.2411904122, 2025.

Barnes, J. M., Dias dos Santos, T., Goldberg, D., Hilmar Gudmundsson, G., Morlighem, M., and De Rydt, J.: The transferability of adjoint inversion products between different ice flow models, The Cryosphere, 15, 1975–2000, https://doi.org/10.5194/tc-15-1975-2021, 2021.

Bett, D. T., Bradley, A. T., Williams, C. R., Holland, P. R., Arthern, R. J., and Goldberg, D. N.: Coupled ice–ocean interactions during future retreat of West Antarctic ice streams in the Amundsen Sea sector, The Cryosphere, 18, 2653–2675, https://doi.org/10.5194/tc-18-2653-2024, 2024.

Campin, J.-M., Heimbach, P., Losch, M., Forget, G., edhill3, Adcroft, A., amolod, Menemenlis, D., dfer22, Hill, C., Jahn, O., Scott, J., stephdut, Mazloff, M., Fox-Kemper, B., antnguyen13, Doddridge, E., Fenty, I., Bates, M., AndrewEichmann-NOAA, Smith, T., mitllheisey, Martin, T., Lauderdale, J., Abernathey, R., samarkhatiwala, Wang, O., hongandyan, Deremble, B., and dngoldberg: dngoldberg/MITgcm: horizontal_coupling_code, https://doi.org/10.5281/zenodo.5777460, 2021.

Campin, J.-M., Heimbach, P., Losch, M., Forget, G., edhill3, Adcroft, A., amolod, Menemenlis, D., dfer22, Jahn, O., Hill, C., Scott, J., dngoldberg, stephdut, Mazloff, M., Fox-Kemper, B., antnguyen13, Doddridge, E., Fenty, I., Bates, M., Smith, T., Wang, O., AndrewEichmann-NOAA, mitllheisey, Lauderdale, J., Martin, T., Abernathey, R., samarkhatiwala, Escobar, I., and averdy: MITgcm/MITgcm: checkpoint69k, https://doi.org/10.5281/zenodo.18371317, 2026.

Chien, Y., Zhou, C., and Riel, B.: Mélange-Driven Coupling Between the Central Pine Island Ice Shelf and the Piglet Glacier Reverses Recent Acceleration Trends, Geophysical Research Letters, 52, e2025GL119 556, https://doi.org/https://doi.org/10.1029/2025GL119556, e2025GL119556 2025GL119556, 2025.

Cornford, S. L., Seroussi, H., Asay-Davis, X. S., Gudmundsson, G. H., Arthern, R., Borstad, C., Christmann, J., Dias dos Santos, T., Feldmann, J., Goldberg, D., et al.: Results of the third Marine Ice Sheet Model Intercomparison Project (MISMIP+), The Cryosphere, pp. 2283–2301, https://doi.org/http://dx.doi.org/10.5194/tc-14-2283-2020, 2020.

Crawford, A. J., Benn, D. I., Todd, J., Åström, J. A., Bassis, J. N., and Zwinger, T.: Marine ice-cliff instability modeling shows mixed-mode ice-cliff failure and yields calving rate parameterization, Nature communications, 12, 2701, 2021.

Cuffey, K. and Paterson, W. S. B.: The Physics of Glaciers, Butterworth Heinemann, Oxford, 4th edn., 2010.

Dansereau, V., Heimbach, P., and Losch, M.: Simulation of subice shelf melt rates in a general circulation model: Velocity-dependent transfer and the role of friction, Journal of Geophysical Research: Oceans, 119, 1765–1790, https://doi.org/10.1002/2013JC008846, 2014.

https://doi.org/10.5194/egusphere-2026-3779
Preprint. Discussion started: 7 July 2026

Davison, B. J., Hogg, A. E., Gourmelen, N., Jakob, L., Wuite, J., Nagler, T., Greene, C. A., Andreasen, J., and Engdahl, M. E.: Annual mass budget of Antarctic ice shelves from 1997 to 2021, Science Advances, 9, eadi0186, 2023.

De Rydt, J. and Naughten, K.: Geometric amplification and suppression of ice-shelf basal melt in West Antarctica, The Cryosphere, 18, 1863–1888, https://doi.org/https://doi.org/10.5194/tc-18-1863-2024, 2024.

DeConto, R. M. and Pollard, D.: Contribution of Antarctica to past and future sea-level rise, Nature, 531, 591–597, https://doi.org/https://doi.org/10.1038/nature17145, 2016.

Dupont, T. K. and Alley, R.: Assessment of the importance of ice-shelf buttressing to ice-sheet flow, Geophys. Res. Lett., 32, L04 503, https://doi.org/http://dx.doi.org/10.1029/2004GL022024, 2005.

Dutrieux, P., De Rydt, J., Jenkins, A., Holland, P., Ha, H., Lee, S., Steig, E., Ding, Q., Abrahamsen, E., and Schröder, M.: Strong Sensitivity of Pine Island Ice-Shelf Melting to Climatic Variability, Science, 343, 174–178, https://doi.org/10.1126/science.1244341, 2014.

Fürst, J. J., Durand, G., Gillet-Chaulet, F., Merino, N., Tavard, L., Mouginot, J., Gourmelen, N., and Gagliardini, O.: Assimilation of Antarctic velocity observations provides evidence for uncharted pinning points, The Cryosphere, 9, 1427–1443, https://doi.org/10.5194/tc-9-1427-2015, 2015.

Fürst, J. J., Durand, G., Gillet-Chaulet, F., Tavard, L., Rankl, M., Braun, M., and Gagliardini, O.: The safety band of Antarctic ice shelves, Nature Climate Change, 6, https://doi.org/10.1038/nclimate2912, 2016.

Gadi, R., Rignot, E., and Menemenlis, D.: Modeling Ice Melt Rates From Seawater Intrusions in the Grounding Zone of Petermann Gletscher, Greenland, Geophysical Research Letters, 50, https://doi.org/10.1029/2023gl105869, 2023.

Gardner, A. S., Moholdt, G., Scambos, T., Fahnstock, M., Ligtenberg, S., Broeke, M. v. d., and Nilsson, J.: Increased West Antarctic and unchanged East Antarctic ice discharge over the last 7 years, The Cryosphere, 12, 521–547, 2018.

Glen, J. W.: The creep of polycrystalline ice, Proc. Royal Soc. of London, Series A, 228, 519–538, 1955.

Goldberg, D.: Code, Input, and Outputs for Century-scale impacts of ice-sheet model initialization on Thwaites Glacier, West Antarctica, https://doi.org/10.5281/zenodo.20796236, 2026.

Goldberg, D. N.: A variationally-derived, depth-integrated approximation to a higher-order glaciological flow model, Journal of Glaciology, 57, 157–170, https://doi.org/http://dx.doi.org/10.3189/002214311795306763, 2011.

Goldberg, D. N. and Heimbach, P.: Parameter and state estimation with a time-dependent adjoint marine ice sheet model, The Cryosphere, 7, 1659–1678, https://doi.org/10.5194/tc-7-1659-2013, 2013.

Goldberg, D. N. and Holland, P.: The relative impacts of initialisation and climate forcing in coupled ice sheet-ocean modelling application to Pope, Smith and Kohler glaciers, Journal of Geophysical Research: Earth Surface, p. e2021JF006570, https://doi.org/10.1029/2021JF006570, 2022.

Goldberg, D. N., Heimbach, P., Joughin, I., and Smith, B.: Committed retreat of Smith, Pope, and Kohler Glaciers over the next 30 years inferred by transient model calibration, The Cryosphere, 9, 2429–2446, https://doi.org/10.5194/tc-9-2429-2015, 2015.

Goldberg, D. N., Snow, K., Holland, P., Jordan, J., Campin, J.-M., Heimbach, P., Arthern, R., and Jenkins, A.: Representing grounding line migration in synchronous coupling between a marine ice sheet model and a z-coordinate ocean model, Ocean Modelling, 125, 45 – 60, https://doi.org/https://doi.org/10.1016/j.ocemod.2018.03.005, 2018.

Goldberg, D. N., Gourmelen, N., Kimura, S., Millan, R., and Snow, K.: How accurately should we model ice shelf melt rates?, Geophysical Research Letters, 46, 189–199, https://doi.org/http://dx.doi.org/10.1029/2018GL080383, 2019.

Goldberg, D. N., Morlighem, M., and Gourmelen, N.: Recent observations of Thwaites Glacier, West Antarctica are consistent with high rates of loss in next 50 years, Geophysical Research Letters, 53, e2025GL118 823, https://doi.org/10.1029/2025GL118823, 2026.

https://doi.org/10.5194/egusphere-2026-3779
Preprint. Discussion started: 7 July 2026

Gourmelen, N., Jakob, L., Holland, P., Dutrieux, P., Goldberg, D., Bevan, S., Luckman, A., and Malczyk, G.: The influence of subglacial lake discharge on Thwaites Glacier ice-shelf melting and grounding-line retreat, Nature Communications, 16, 2272, https://doi.org/10.1038/s41467-025-57417-1, 2025.

Greve, R. and Blatter, H.: Dynamics of Ice Sheets and Glaciers, Springer, Dordrecht, 2009.

Grosfeld, K., Gerdes, R., and Determann, J.: Thermohaline circulation and interaction between ice shelf cavities and the adjacent open ocean, Journal of Geophysical Research, 102, 15 595–15 610, 1997.

Gudmundsson, G. H., Barnes, J. M., Goldberg, D., and Morlighem, M.: Limited impact of Thwaites Ice Shelf on future ice loss from Antarctica, Geophysical Research Letters, 50, e2023GL102 880, https://doi.org/10.1029/2023GL102880, 2023.

Haigh, M., Holland, P. R., Harrison, T. C., and Dutrieux, P.: Wind-driven coastal polynya variability drives decadal ice-shelf melt variability in the Amundsen Sea, Geophysical Research Letters, 53, e2025GL118 546, https://doi.org/10.1029/2025GL118546, 2026.

Hill, E. A., Urruty, B., Reese, R., Garbe, J., Gagliardini, O., Durand, G., Gillet-Chaulet, F., Gudmundsson, G. H., Winkelmann, R., Chekki, M., Chandler, D., and Langebroek, P. M.: The stability of present-day Antarctic grounding lines – Part 1: No indication of marine ice sheet instability in the current geometry, The Cryosphere, 17, 3739–3759, https://doi.org/10.5194/tc-17-3739-2023, 2023.

Holland, D. M. and Jenkins, A.: Modelling thermodynamic ice-ocean interactions at the base of an ice shelf, J. Phys. Ocean., 29, 1787–1800, https://doi.org/https://doi.org/10.1175/1520-0485(1999)029, 1999.

Holland, D. M., Thomas, R. H., de Young, B., Ribergaard, M., and Lyberth, B.: Acceleration of Jakobshavn Isbrae triggered by warm subsurface ocean waters, Nat. Geosci., 1, 659–664, 2008.

Holland, P. R., Bevan, S. L., and Luckman, A. J.: Strong ocean melting feedback during the recent retreat of Thwaites Glacier, Geophysical Research Letters, 50, e2023GL103 088, https://doi.org/10.1029/2023GL103088, 2023.

Jenkins, A., Nicholls, K. W., and Corr, H. F. J.: Observation and Parameterization of Ablation at the Base of Ronne Ice Shelf, Antarctica, Journal of Physical Oceanography, 40, 2298 – 2312, https://doi.org/10.1175/2010JPO4317.1, 2010.

Jenkins, A., Shoosmith, D., Dutrieux, P., Jacobs, S., Kim, T. W., Le, S. H., Ha, H. K., and Stammerjohn, S.: West Antarctic Ice Sheet retreat in the Amundsen Sea driven by decadal oceanic variability, Nat. Geoscience, 11, 733–738, https://doi.org/https://doi.org/10.1038/s41561-018-0207-4DO, 2018.

Jordan, J. R., Holland, P. R., Goldberg, D., Snow, K., Arthern, R., Campin, J. M., Heimbach, P., and Jenkins, A.: Ocean-Forced Ice-Shelf Thinning in a Synchronously Coupled Ice-Ocean Model, Journal of Geophysical Research: Oceans, pp. 864–882, https://doi.org/10.1002/2017JC013251, 2017.

Jordan, T., Ferraccioli, F., Vaughan, D., Holt, J., Corr, H., Blankenship, D., and Diehl, T.: Aerogravity evidence for major crustal thinning under the Pine Island Glacier region (West Antarctica), GSA Bulletin, 122, 714–726, https://doi.org/10.1130/B26417.1, 2010.

Joughin, I., Smith, B. E., and Medley, B.: Marine Ice Sheet Collapse Potentially Under Way for the Thwaites Glacier Basin, West Antarctica, Science, 344, 735–738, https://doi.org/10.1126/science.1249055, 2014.

Joughin, I., Smith, B. E., and Schoof, C. G.: Regularized Coulomb friction laws for ice sheet sliding: Application to Pine Island Glacier, Antarctica, Geophysical research letters, 46, 4764–4771, https://doi.org/10.1029/2019GL082526, 2019.

Joughin, I., Shapero, D., Smith, B., Dutrieux, P., and Barham, M.: Ice-shelf retreat drives recent Pine Island Glacier speedup, Science Advances, 7, eabg3080, https://doi.org/DOI: 10.1126/sciadv.abg3080, 2021.

Jourdain, N. C., Mathiot, P., Burgard, C., Caillet, J., and Kittel, C.: Ice Shelf Basal Melt Rates in the Amundsen Sea at the End of the 21st Century, Geophysical Research Letters, 49, e2022GL100 629, https://doi.org/https://doi.org/10.1029/2022GL100629, e2022GL100629 2022GL100629, 2022.

https://doi.org/10.5194/egusphere-2026-3779
Preprint. Discussion started: 7 July 2026

Kay, J. E., Deser, C., Phillips, A., Mai, A., Hannay, C., Strand, G., Arblaster, J. M., Bates, S., Danabasoglu, G., Edwards, J., et al.: The Community Earth System Model (CESM) large ensemble project: A community resource for studying climate change in the presence of internal climate variability, Bulletin of the American Meteorological Society, 96, 1333–1349, https://doi.org/https://doi.org/10.1175/BAMS-D-13-00255.1, 2015.

Lhermitte, S., Sun, S., Shuman, C., Wouters, B., Pattyn, F., Wuite, J., Berthier, E., and Nagler, T.: Damage accelerates ice shelf instability and mass loss in Amundsen Sea Embayment, Proceedings of the National Academy of Sciences, 117, 24 735–24 741, 2020.

Lipscomb, W. H., Price, S. F., Hoffman, M. J., Leguy, G. R., Bennett, A. R., Bradley, S. L., Evans, K. J., Fyke, J. G., Kennedy, J. H., Perego, M., et al.: Description and evaluation of the Community Ice Sheet Model (CISM) v2.1, Geoscientific Model Development, 12, 387–424, https://doi.org/http://dx.doi.org/10.5194/gmd-12-387-2019, 2019.

Losch, M. and Heimbach, P.: Adjoint sensitivity of an ocean general circulation model to bottom topography, J. Phys. Ocean., 37, 377–393, https://doi.org/10.1175/JPO3017.1, 2007.

Lowry, D. P., Krapp, M., Golledge, N. R., and Alevropoulos-Borrill, A.: The influence of emissions scenarios on future Antarctic ice loss is unlikely to emerge this century, Communications Earth & Environment, 2, 221, https://doi.org/https://doi.org/10.1038/s41467-021-22259-0, 2021.

Marshall, J., Hill, C., Perelman, L., and Adcroft, A.: Hydrostatic, quasi-hydrostatic, and nonhydrostatic ocean modeling, Journal of Geophysical Research: Oceans, 102, 5733–5752, https://doi.org/10.1029/96JC02776, 1997.

Milillo, P., Rignot, E., Rizzoli, P., Scheuchl, B., Mouginot, J., Bueso-Bello, J., and Prats-Iraola, P.: Heterogeneous retreat and ice melt of Thwaites Glacier, West Antarctica, Science advances, 5, eaau3433, https://doi.org/http://dx.doi.org/10.1126/sciadv.aau3433, 2019.

Morlighem, M.: MEaSUREs BedMachine Antarctica, Version 3, https://doi.org/10.5067/FPSU0V1MWUB6, 2022.

Morlighem, M. and Goldberg, D. N.: Data assimilation in Glaciology, in: Applications of Data Assimilation and Inverse Problems in the Earth Sciences, edited by Ismail-Zadeh, A., Castelli, F., Jones, D., and Sanchez, S., chap. 6, pp. 93–110, Cambridge University Press, Cambridge, 2023.

Morlighem, M., Rignot, E., Binder, T., Blankenship, D., Drews, R., Eagles, G., Eisen, O., Ferraccioli, F., Forsberg, R., Fretwell, P., et al.: Deep glacial troughs and stabilizing ridges unveiled beneath the margins of the Antarctic ice sheet, Nature Geoscience, 13, 132–137, https://doi.org/http://dx.doi.org/10.1038/s41561-019-0510-8, 2020a.

Morlighem, M., Rignot, E., Binder, T., Blankenship, D., Drews, R., et al.: Deep glacial troughs and stabilizing ridges unveiled beneath the margins of the Antarctic ice sheet, Nature Geoscience, 13, 132–137, https://doi.org/10.1038/s41561-019-0510-8, 2020b.

Morlighem, M., Goldberg, D., Barnes, J. M., Bassis, J. N., Benn, D. I., Crawford, A. J., Gudmundsson, G. H., and Seroussi, H.: The West Antarctic Ice Sheet may not be vulnerable to marine ice cliff instability during the 21st century, Science Advances, 10, eado7794, https://doi.org/10.1126/sciadv.ado7794, 2024.

Mouginot, J., Scheuchl, B., and Rignot, E.: MEaSUREs Antarctic Boundaries for IPY 2007-2009 from Satellite Radar, Version 2, https://doi.org/10.5067/AXE4121732AD, 2017.

Naughten, K. A., Holland, P. R., and De Rydt, J.: Unavoidable future increase in West Antarctic ice-shelf melting over the twenty-first century, Nature Climate Change, 13, 1222–1228, https://doi.org/10.1038/s41558-023-01818-x, 2023a.

Naughten, K. A., Holland, P. R., and Rydt, J. D.: Unavoidable future increase in West Antarctic ice-shelf melting over the twenty-first century, Nature Climate Change, https://doi.org/10.1038/s41558-023-01818-x, 2023b.

Nick, F., Van Der Veen, C., Vieli, A., and Benn, D.: A physically based calving model applied to marine outlet glaciers and implications for the glacier dynamics, Journal of Glaciology, 56, 781–794, https://doi.org/10.3189/002214310794457344, 2010.

https://doi.org/10.5194/egusphere-2026-3779
Preprint. Discussion started: 7 July 2026

Paolo, F. S., Fricker, H. A., and Padman, L.: Volume loss from Antarctic ice shelves is accelerating, Science, 348, 327–331, https://doi.org/10.1126/science.aaa0940, 2015.

Pritchard, H. D., Ligtenberg, S. R. M., Fricker, H. A., Vaughan, D. G., van den Broeke, M. R., and Padman, L.: Antarctic ice-sheet loss driven by basal melting of ice shelves, Nature, 484, 502–505, https://doi.org/doi:10.1038/nature10968, 2012.

Reed, B., Green, J. M., Jenkins, A., and Gudmundsson, G. H.: Recent irreversible retreat phase of Pine Island Glacier, Nature Climate Change, 14, 75–81, https://doi.org/10.1038/s41558-023-01887-y, 2024.

Reed, B., De Rydt, J., Naughten, K. A., and Goldberg, D. N.: Calibration of a coupled ice sheet-ocean model using observations of ice dynamics and basal melt in West Antarctica, EGUsphere, 2026, 1–39, https://doi.org/10.5194/egusphere-2026-931, 2026.

Reese, R., Albrecht, T., Mengel, M., Asay-Davis, X., and Winkelmann, R.: Antarctic sub-shelf melt rates via PICO, The Cryosphere, 12, 1969–1985, 2018a.

Reese, R., Gudmundsson, G. H., Levermann, A., and Winkelmann, R.: The far reach of ice-shelf thinning in Antarctica, Nature Climate Change, 8, 53–57, https://doi.org/https://doi.org/10.1038/s41558-017-0020-x, 2018b.

Reese, R., Garbe, J., Hill, E. A., Urruty, B., Naughten, K. A., Gagliardini, O., Durand, G., Gillet-Chaulet, F., Gudmundsson, G. H., Chandler, D., Langebroek, P. M., and Winkelmann, R.: The stability of present-day Antarctic grounding lines – Part 2: Onset of irreversible retreat of Amundsen Sea glaciers under current climate on centennial timescales cannot be excluded, The Cryosphere, 17, 3761–3783, https://doi.org/10.5194/tc-17-3761-2023, 2023.

Rignot, E., Mouginot, J., and Scheuchl, B.: Ice Flow of the Antarctic Ice Sheet, Science, 333, 1427–1430, https://doi.org/10.1126/science.1208336, 2011.

Rignot, E., Mouginot, J., and Scheuchl, B.: MEaSUREs InSARBased Antarctica Ice Velocity Map, Version 2, Boulder, Colorado USA, NASA National Snow and Ice Data Center Distributed Active Archive Center, https://doi.org/10.5067/D7GK8F5J8M8R, 2017.

Rignot, E., Mouginot, J., Scheuchl, B., Van Den Broeke, M., Van Wessem, M. J., and Morlighem, M.: Four decades of Antarctic Ice Sheet mass balance from 1979–2017, Proceedings of the National Academy of Sciences, 116, 1095–1103, https://doi.org/10.1073/pnas.1904242116, 2019.

Robinson, A., Goldberg, D., and Lipscomb, W. H.: A comparison of the stability and performance of depth-integrated ice-dynamics solvers, The Cryosphere, 16, 689–709, https://doi.org/10.5194/tc-16-689-2022, 2022.

Scambos, T. A., Bell, R. E., Alley, R. B., Anandakrishnan, S., Bromwich, D., Brunt, K., Christianson, K., Creyts, T., Das, S., DeConto, R., et al.: How much, how fast?: A science review and outlook for research on the instability of Antarctica's Thwaites Glacier in the 21st century, Global and Planetary Change, 153, 16–34, https://doi.org/10.1016/j.gloplacha.2017.04.008, 2017.

Scheuchl, B., Mouginot, J., Rignot, E., Morlighem, M., and Khazendar, A.: Grounding line retreat of Pope, Smith, and Kohler Glaciers, West Antarctica, measured with Sentinel-1a radar interferometry data, Geophysical Research Letters, 43, 8572–8579, https://doi.org/10.1002/2016GL069287, 2016.

Schoof, C.: Marine ice sheet dynamics. Part I. The case of rapid sliding, J. Fluid Mech., 573, 27–55, https://doi.org/http://dx.doi.org/10.1017/S0022112006003570, 2007.

Schwans, E., Parizek, B. R., Alley, R. B., Anandakrishnan, S., and Morlighem, M. M.: Model insights into bed control on retreat of Thwaites Glacier, West Antarctica, Journal of Glaciology, 69, 1241–1259, https://doi.org/10.1017/jog.2023.13, 2023.

Seroussi, H., Pelle, T., Lipscomb, W. H., Abe-Ouchi, A., Albrecht, T., Alvarez-Solas, J., Asay-Davis, X., Barre, J.-B., Berends, C. J., Bernales, J., et al.: Evolution of the Antarctic Ice Sheet over the next three centuries from an ISMIP6 model ensemble, Earth's Future, 12, e2024EF004 561, https://doi.org/10.1029/2024EF004561, 2024.

https://doi.org/10.5194/egusphere-2026-3779
Preprint. Discussion started: 7 July 2026

Shepherd, A., Wingham, D. J., and Rignot, E.: Warm ocean is eroding West Antarctic Ice Sheet, Geophys. Res. Lett., 31, L23 402, https://doi.org/http://dx.doi.org/10.1029/2004GL021106, 2004.

Shepherd, A., Gilbert, L., Muir, A. S., Konrad, H., McMillan, M., Slater, T., Briggs, K. H., Sundal, A. V., Hogg, A. E., and Engdahl, M. E.: Trends in Antarctic Ice Sheet elevation and mass, Geophysical Research Letters, 46, 8174–8183, https://doi.org/http://dx.doi.org/10.1029/2019GL082182, 2019.

Snow, K., Goldberg, D., Holland, P. R., Jordan, J. R., Arthern, R. J., and Jenkins, A.: The Response of Ice Sheets to Climate Variability, Geophysical Research Letters, 44, 11,878–11,885, https://doi.org/10.1002/2017GL075745, 2017.

Stern, A. A., Adcroft, A. J., Sergienko, O. V., and Marques, G. M.: Modeling tabular icebergs submerged in the ocean, Journal of Advances in Modeling Earth Systems, 9, 1948 – 1972, https://doi.org/10.1002/2017MS001002, 2017.

Surawy-Stepney, T., Hogg, A. E., Cornford, S. L., and Davison, B. J.: Episodic dynamic change linked to damage on the Thwaites Glacier Ice Tongue, Nature Geoscience, 16, https://doi.org/10.1038/s41561-022-01097-9, 2023.

Taylor, K. E., Stouffer, R. J., and Meehl, G. A.: An Overview of CMIP5 and the Experiment Design, Bull. Amer. Met. Soc., 93, 485–498, https://doi.org/http://dx.doi.org/10.1175/BAMS-D-11-00094.1, 2012.

Turner, K., Naughten, K., Holland, P., and Naveira Garabato, A.: Modeled centennial ocean warming in the Amundsen Sea driven by thermodynamic atmospheric changes, not winds, Geophysical Research Letters, 52, e2024GL112 287, https://doi.org/https://doi.org/10.1029/2024GL112287, 2025.

van den Akker, T., Lipscomb, W. H., Leguy, G. R., van de Berg, W. J., and van de Wal, R. S. W.: Competing processes determine the long-term impact of basal friction parameterizations for Antarctic mass loss, The Cryosphere, 20, 1217–1235, https://doi.org/10.5194/tc-20-1217-2026, 2026.

Van Liefferinge, B. and Pattyn, F.: Using ice-flow models to evaluate potential sites of million year-old ice in Antarctica, Climate of the Past Discussions, 9, https://doi.org/http://dx.doi.org/10.5194/cp-9-2335-2013, 2013.

Van Wessem, J., Reijmer, C., Morlighem, M., Mouginot, J., Rignot, E., Medley, B., Joughin, I., Wouters, B., Depoorter, M., Bamber, J., and et al.: Improved representation of East Antarctic surface mass balance in a regional atmospheric climate model, Journal of Glaciology, 60, 761–770, https://doi.org/10.3189/2014JoG14J051, 2014.

Wåhlin, A., Yuan, X., Björk, G., and Nohr, C.: Inflow of warm circumpolar deep water in the central Amundsen shelf, Journal of physical oceanography, 40, 1427–1434, https://doi.org/https://doi.org/10.1175/2010JPO4431.1, 2010.

Walker, D. P., Jenkins, A., Assmann, K., Shoosmith, D., and Brandon, M.: Oceanographic observations at the shelf break of the Amundsen Sea, Antarctica, Journal of Geophysical Research: Oceans, 118, 2906–2918, https://doi.org/10.1002/jgrc.20212, 2013.

Weertman, J.: Stability of the junction of an ice sheet and an ice shelf, Journal of Glaciology, 13, 3–11, 1974.

Wilner, J. A., Morlighem, M., and Cheng, G.: Evaluation of four calving laws for Antarctic ice shelves, The Cryosphere, 17, 4889–4901, https://doi.org/10.5194/tc-17-4889-2023, 2023.

Yung, C. K., Asay-Davis, X. S., Adcroft, A., Bull, C. Y. S., De Rydt, J., Dinniman, M. S., Galton-Fenzi, B. K., Goldberg, D., Gwyther, D. E., Hallberg, R., Harrison, M., Hattermann, T., Holland, D. M., Holland, D., Holland, P. R., Jordan, J. R., Jourdain, N. C., Kusahara, K., Marques, G., Mathiot, P., Menemenlis, D., Morrison, A. K., Nakayama, Y., Sergienko, O., Smith, R. S., Stern, A., Timmermann, R., and Zhou, Q.: Results of the second Ice Shelf–Ocean Model Intercomparison Project (ISOMIP+), The Cryosphere, 20, 2053–2088, https://doi.org/10.5194/tc-20-2053-2026, 2026.

https://doi.org/10.5194/egusphere-2026-3779
Preprint. Discussion started: 7 July 2026

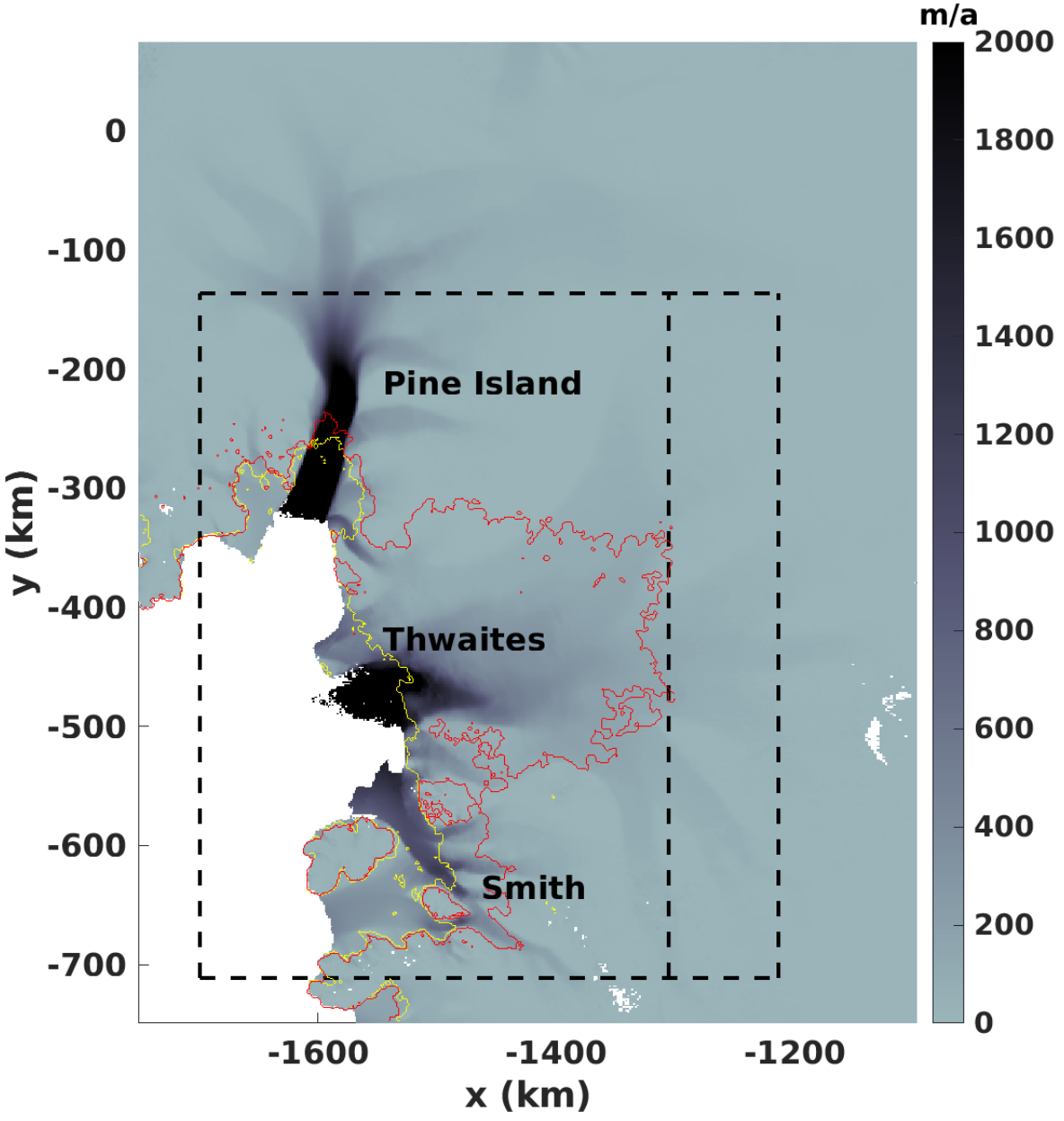

Figure 1. The figure shows the extent of the ice-sheet model (*ICE*), while dashed lines give that of the ocean model (*OCE*, see Section 2.3). Shading is observed ice-sheet velocity (Rignot et al., 2017). The yellow contour is the grounding line as given by Morlighem et al. (2020a), while the red contour is that of the final time of the **TCBase** experiment. Both **TC85** and **Snap85** are run entirely with the smaller of the ocean domains while the ocean domains of **TCBase** and **SnapBase** are expanded to the larger one at 2200.

https://doi.org/10.5194/egusphere-2026-3779
Preprint. Discussion started: 7 July 2026

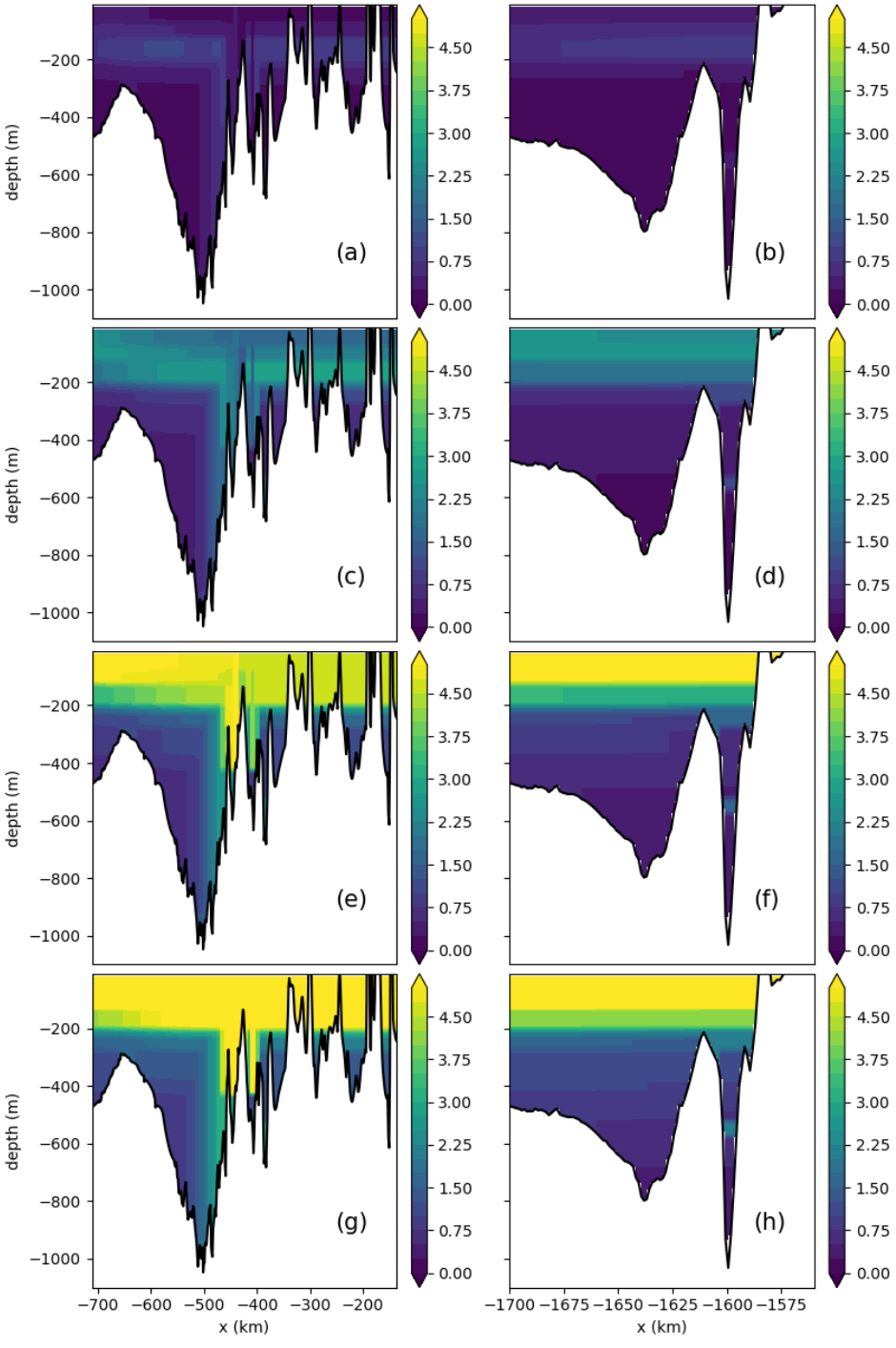

Figure 2. Downscaled temperature anomalies at domain boundaries from the ISMIP6-2300 CESM2 forcing which are added to the 2000-2010 climatology from Naughten et al. (2023a). (a,c,e,g) temperatures at the northern (left) domain boundary in years 2050, 2100, 2150, 2200, respectively. (b,d,f,h) similar for the western (bottom) boundary.

https://doi.org/10.5194/egusphere-2026-3779
Preprint. Discussion started: 7 July 2026

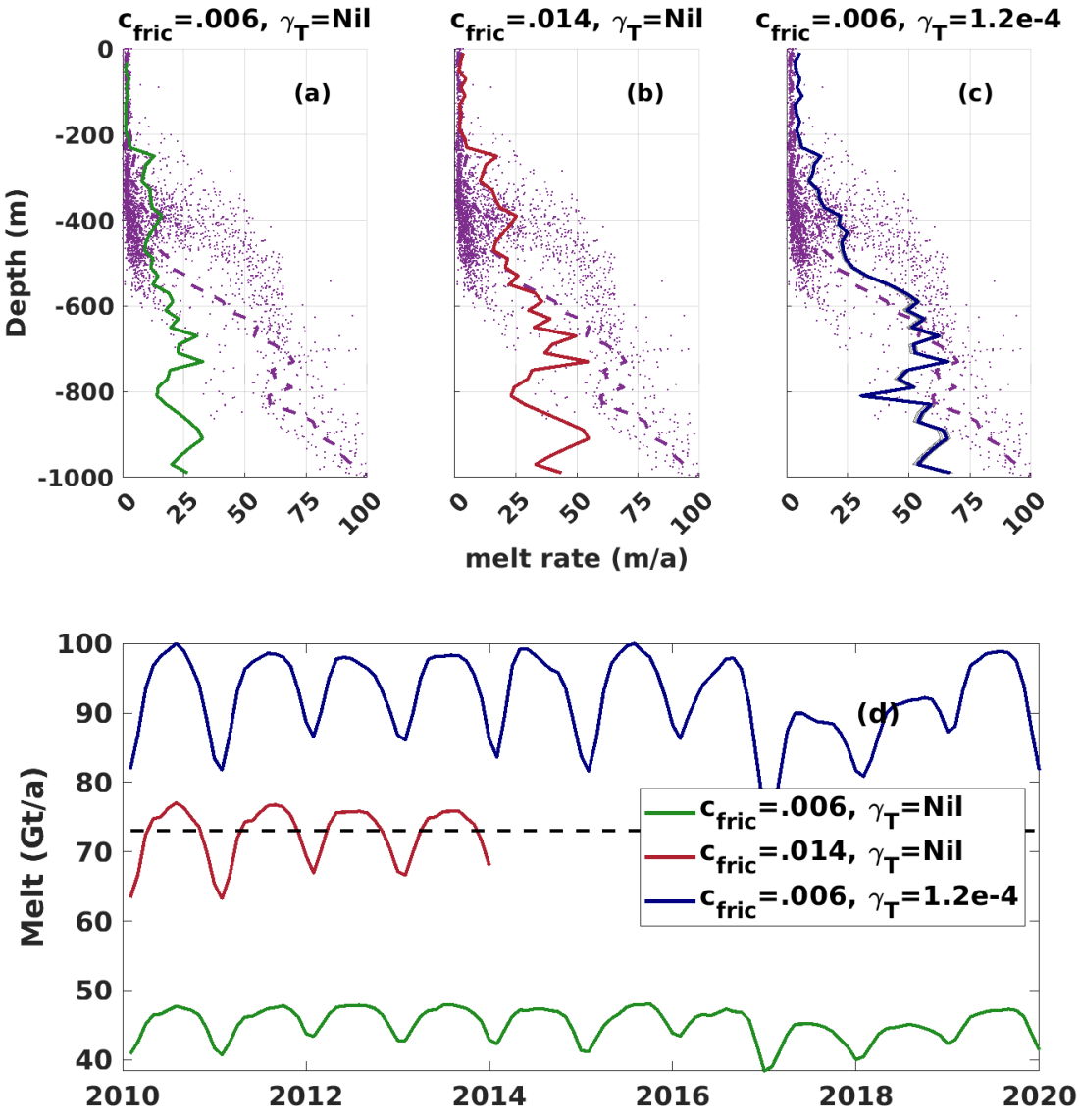

Figure 3. (a)-(c) compare melt-depth relationships for Pine Island (black lines) against observed (Gourmelen et al., 2025, , purple lines) for different melt parameters. The point cloud corresponds to observations as well. The melt-depth curves (modelled and observed) are found by averaging melt rate in 20 m depth bins over the cavity, and averaging between 2010 and 2020 (the approximate period of the observed melt). "γ_T=Nil" indicates that Dansereau et al. (2014) melt formulation is used everywhere. The "$c_{fric} = .014$, γ_T=Nil" is averaged only over 2010-2014, as its run was truncated. (d) Area-integrated melt over time corresponding to the mean profiles in (a)-(c), compared with that of the observed melt (dashed line).

https://doi.org/10.5194/egusphere-2026-3779
Preprint. Discussion started: 7 July 2026

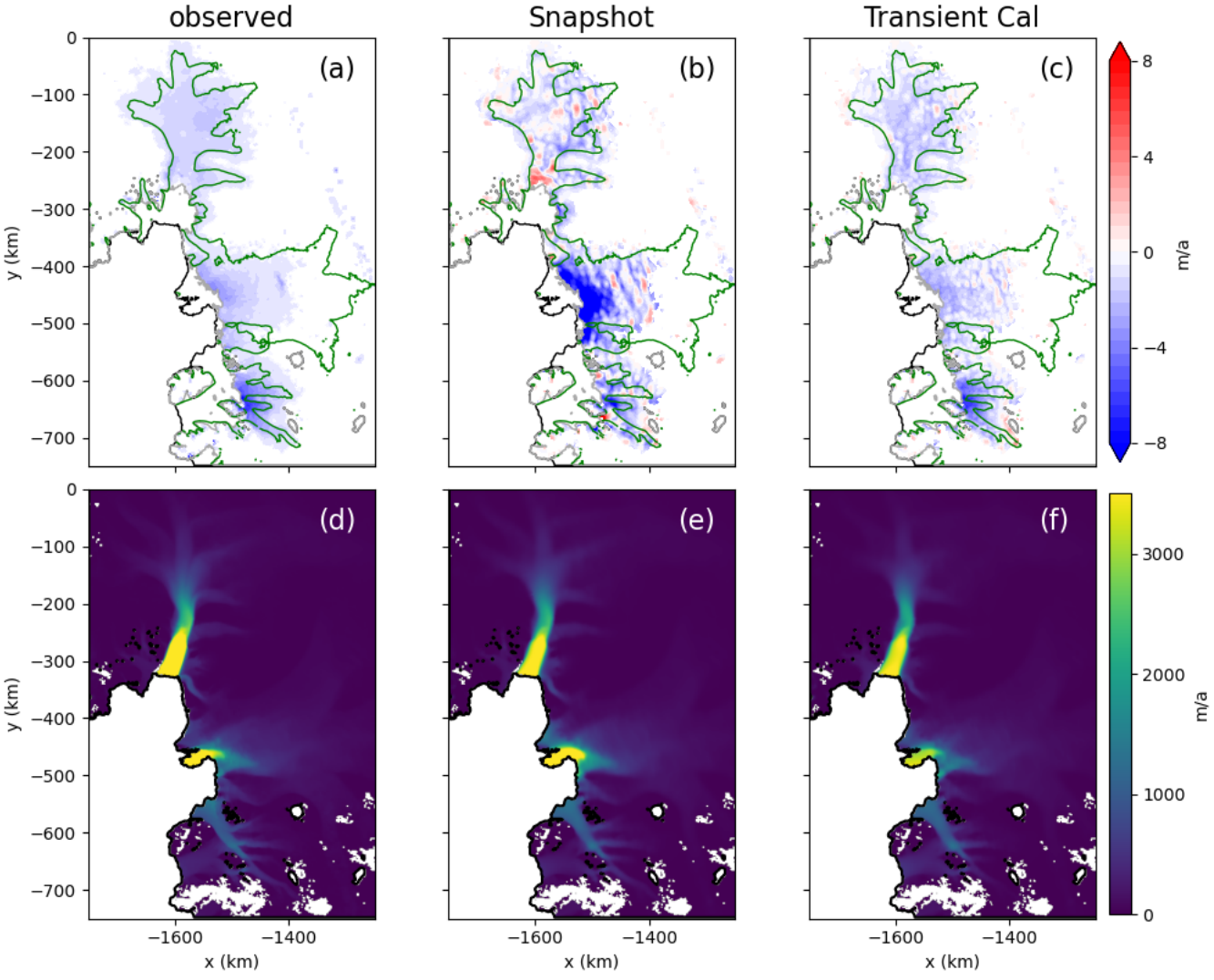

Figure 4. (a)-(c) Grounded surface elevation change in the Amundsen region, for (a) observations, (b) Snapshot calibration, and (c) Transient Calibration. Values are masked where observed thinning is less than 0.5 m/a. The black line is BedMachine ice extent, and the green line is the MEaSUREs 100 m/a velocity contour. (d) Observed surface speed (Rignot et al., 2017). (e) surface speed in Snapshot calibration. (f) surface speed after 1 year in Transient calibration.

https://doi.org/10.5194/egusphere-2026-3779
Preprint. Discussion started: 7 July 2026

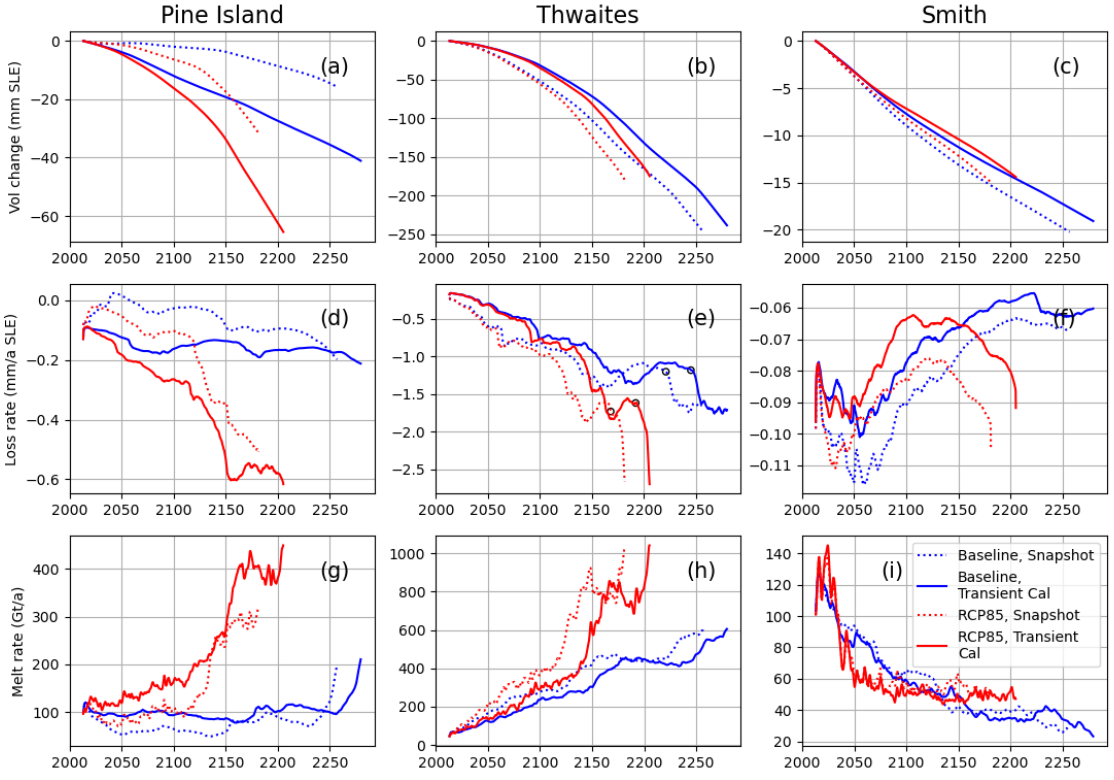

Figure 5. (a)-(c) Change in Volume above Floatation (V_{af}, expressed in mm sea level) in the four coupled experiments for Pine Island, Thwaites and Smith catchments (see Section 3 for catchment definitions). (d)-(f) Rate of change of V_{af} for each experiment in each catchment. The small black circles in (e) indicate the timing of the respective grounding line contour in Fig. 7b. Area-integrated melt for each experiment in each catchment. A Gaussian smoothing kernel with 6-month standard deviation is applied to melt rates.

https://doi.org/10.5194/egusphere-2026-3779
Preprint. Discussion started: 7 July 2026

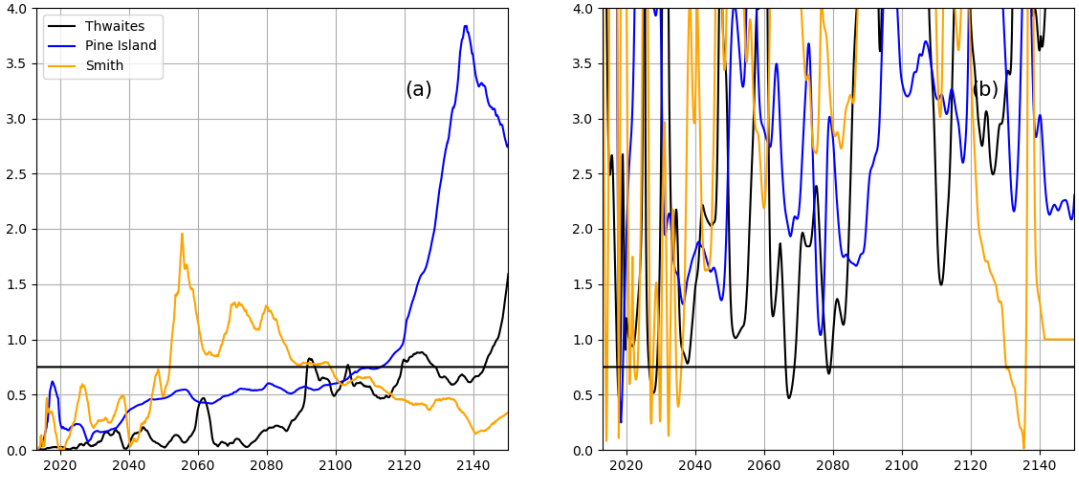

Figure 6. "Emergence" of climate forcing dependence (Eq. 5) in terms of V_{af} loss rate (a) and melt rate (b).

https://doi.org/10.5194/egusphere-2026-3779
Preprint. Discussion started: 7 July 2026

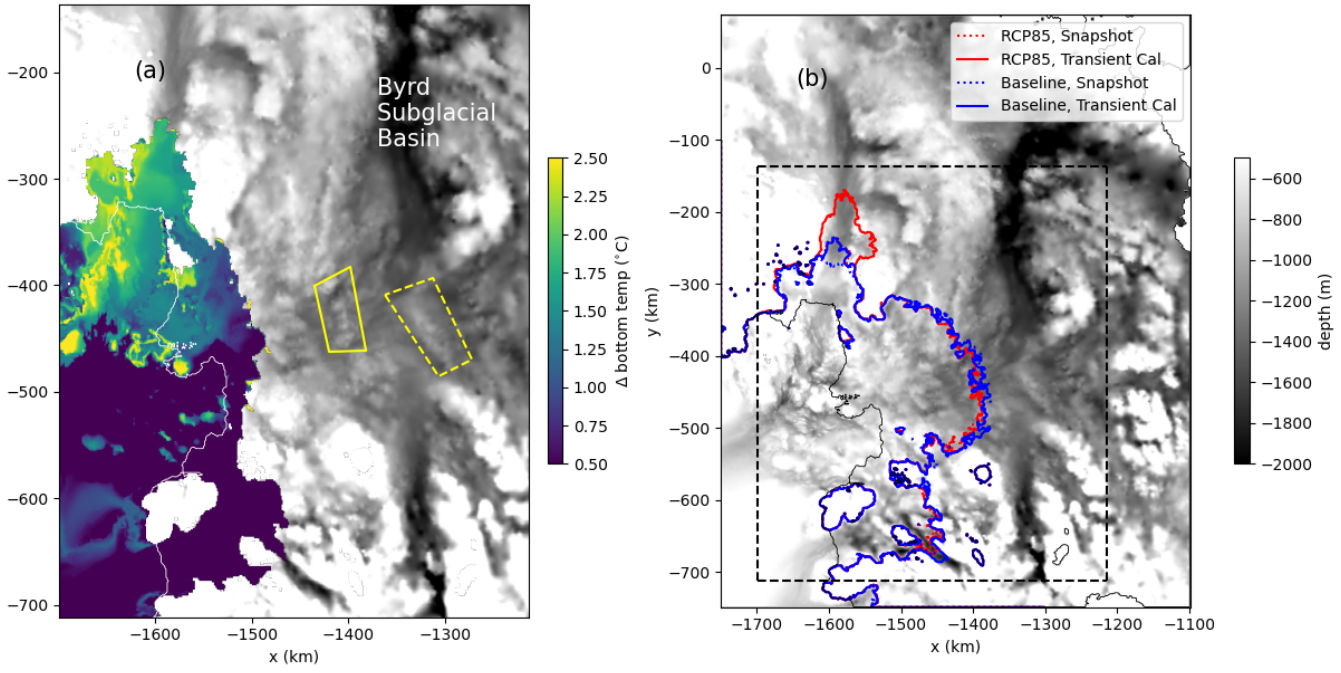

Figure 7. (a) Colored shading is bottom temperature in **TC85** minus bottom temperature in **TCBase** in year 2100, over the common ocean-covered area. The thin white contour shows ice extent in BedMachine-Antarctica (as does the thin black contour in (b)). The solid yellow polygon indicates Upper Thwaites Ridge and the dashed yellow polygon is an "Unnamed" ridge. The extent of (a) is shown in the dashed box in (b). (b) Contours show the grounding lines for each coupled simulation at the time when loss rates are temporarily slowed (Fig. 5e), corresponding to 2168 for **Snap85**; 2192 for **TC85**; 2221 for **SnapBase**; and 2245 for **TCBase** (see Fig. 5e). Gray shading is model bathymetry.

https://doi.org/10.5194/egusphere-2026-3779
Preprint. Discussion started: 7 July 2026

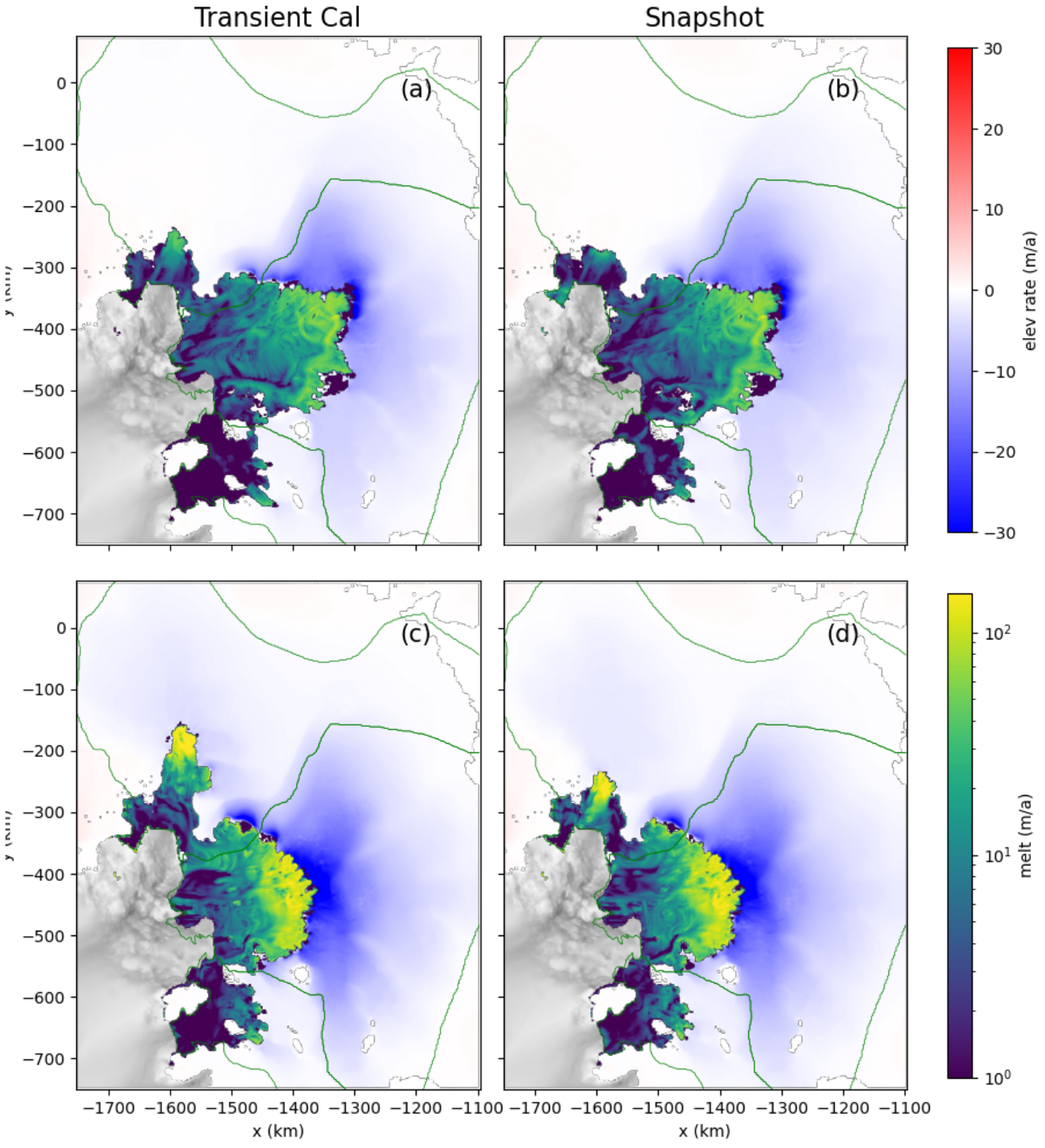

Figure 8. Melt rates and grounded thinning rates at the point of model failure in the respective experiments: **TCBase** (a), **SnapBase** (b), **TC85** (c), and **Snap85** (d). Green contours denote glacial catchments. Note the logarithmic color scale for melt rates.

https://doi.org/10.5194/egusphere-2026-3779
Preprint. Discussion started: 7 July 2026

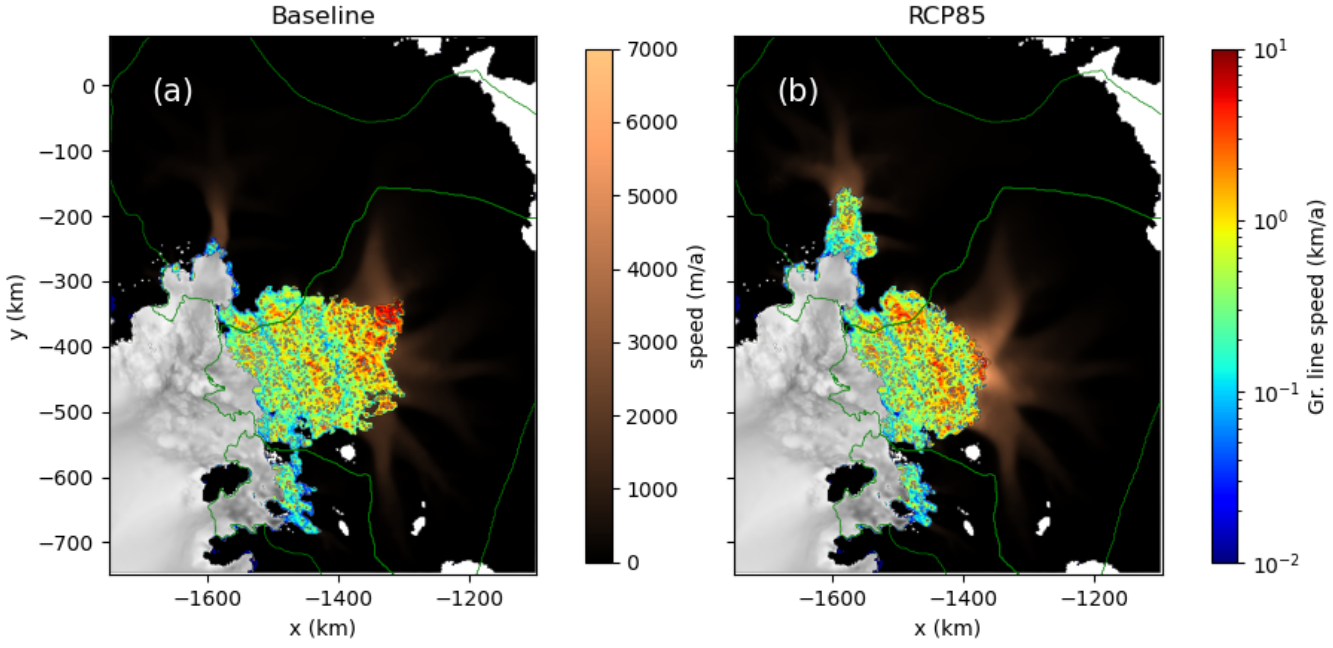

Figure 9. Grounding line "speed" (Eq. 6) and grounded-ice speed in the Transiently Calibrated experiments: **TCBase** (a), **TC85** (b). Green contours denote catchments. Note the logarithmic color scale for grounding line speed.

https://doi.org/10.5194/egusphere-2026-3779
Preprint. Discussion started: 7 July 2026

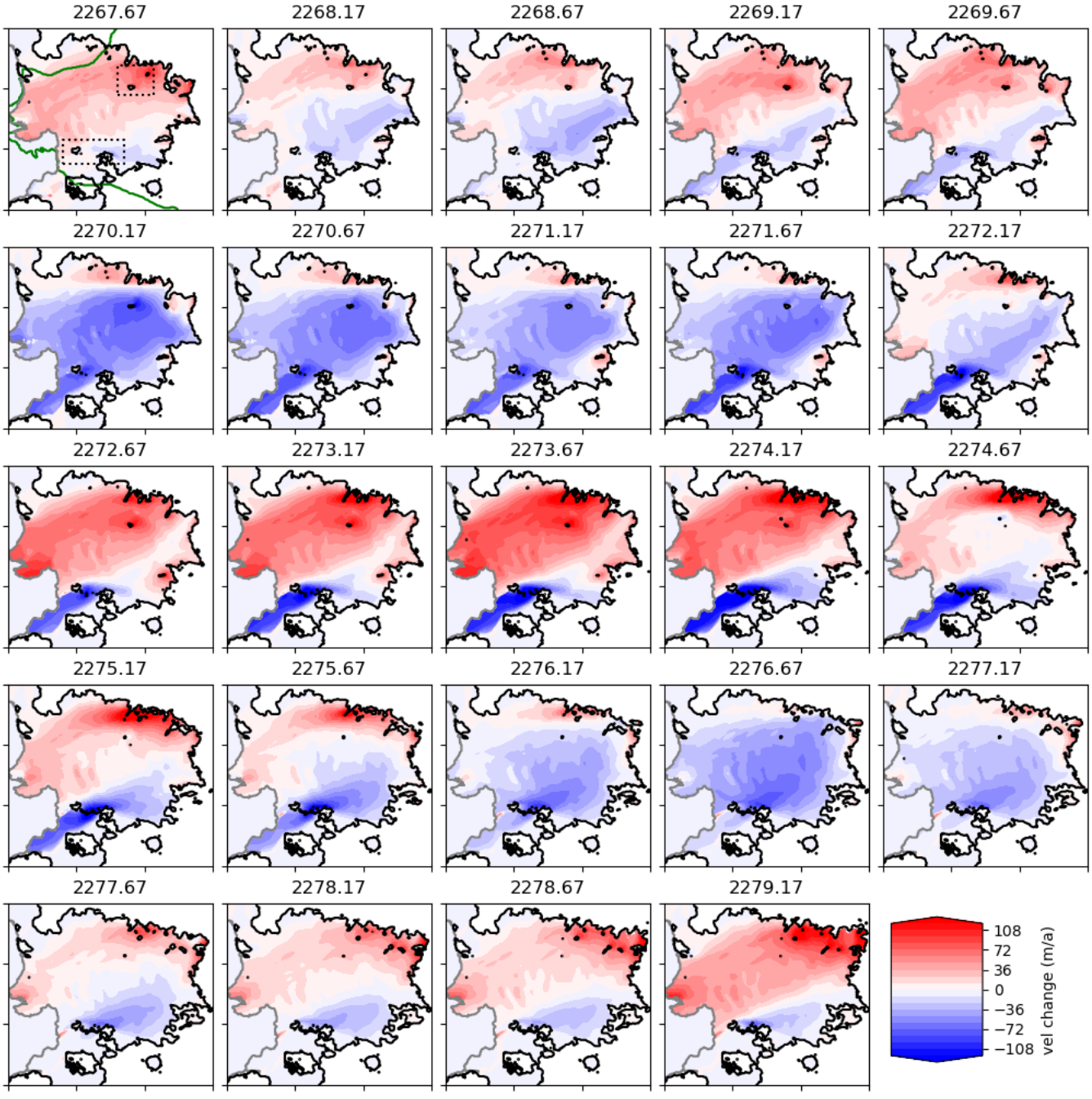

Figure 10. Changes in speed in the **TCBase** experiment; each panel is speed change over the previous 6 months. The thin black line shows the BedMachine ice extent, and the thick black line shows the grounding line. The initial panel shows the demarcation of the Thwaites catchment (green contour) and the locations of the pinning points examined in Fig. 11.

https://doi.org/10.5194/egusphere-2026-3779
Preprint. Discussion started: 7 July 2026

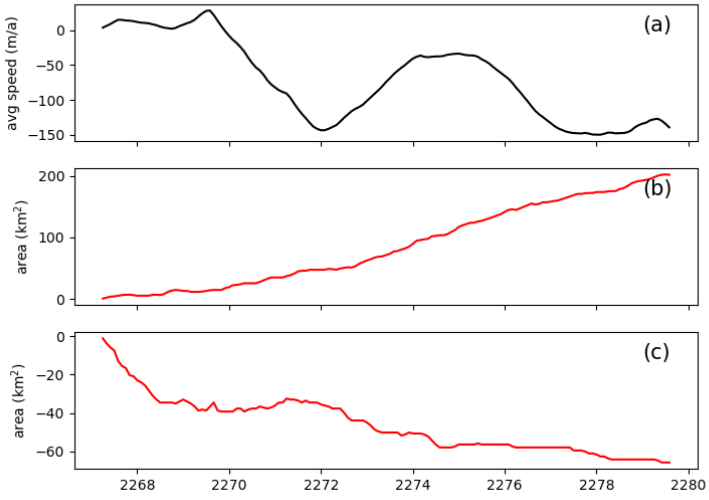

Figure 11. (a) The area-averaged ice-shelf speed within the Thwaites catchment in the **TCBase** over the period shown in Fig. 10, relative to Feb. 2267. (b) The grounded area shown in the western box in Fig. 11, relative to Feb. 2267. (c) As in (b), but for the eastern box.

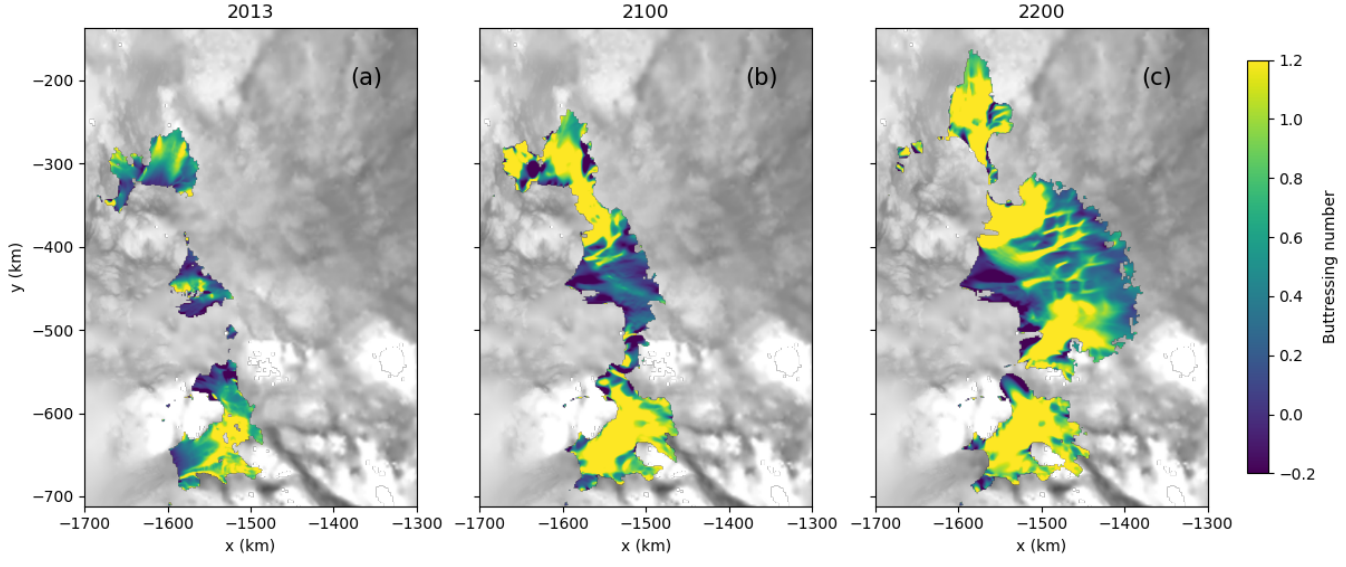

Figure 12. The Buttressing number $1 - r_B$ (Eq. 7) calculated over ASE ice shelves in 2013 (a), 2100 (b), and 2200 (c) for the **TC85** experiment. Values are masked for shelf thickness below 30 m. A value of $1 - r_B$ close to 1 implies high buttressing.